Alberto F. Maroto[1,2,3], Mireia Borrajo[1,2,3], Sílvia Prades[1], Àngela Callejo[4,5], Emilio Amilibia[4,5], Marta Pérez-Grau[4,5], Francesc Roca-Ribas[4,5], Elisabeth Castellanos[5,6], Alejandro Barrallo-Gimeno[1,2,3], Jordi Llorens[1,2,3]

The vestibular calyceal junction is dismantled in response to diverse injuring stimuli in rats and humans

[1] Departament de Ciències Fisiològiques, Universitat de Barcelona (UB), Feixa Llarga s/n, 08907 l'Hospitalet de Llobregat, Catalunya, Spain.

[2] Institut de Neurociències, Universitat de Barcelona (UB), Barcelona, Catalunya, Spain.

[3] Institut d'Investigació Biomèdica de Bellvitge (IDIBELL), 08907 l'Hospitalet de Llobregat, Catalunya, Spain.

[4] Servei d'Otorinolaringologia, Hospital Universitari Germans Trias i Pujol, Badalona, Catalunya, Spain.

[5] CSUR Phakomatoses Multidisciplinary Clinics HUGTIP-ICO-IGTP, Barcelona, Catalunya, Spain.

[6] Clinical Genomics Research Group, Institut de Recerca Germans Trias i Pujol (IGTP), Badalona, Catalunya, Spain.

Corresponding author: Prof. Jordi Llorens, Ph.D.; e-mail: jllorens@ub.edu; Ph: +34934024277

E-mail addresses and ORCID codes:

A.F.M.: albertomaroto@hotmail.com; 0000-0001-8265-4902

M.B.: mborrajoarjona@ub.edu; 0000-0003-2126-5713

S.P.: silvia.prab@gmail.com; 0000-0001-8561-2919

A.C.: angelacallejo@gmail.com; 0000-0003-3820-7405

E.A.: emilioamilibia@gmail.com; 0000-0003-0587-7891

M.P.G.: martaperezgrau@gmail.com; 0000-0003-4630-0116

F. R.R.: francescrocaribas@gmail.com; 0000-0001-6620-8216

E.C.: ecastellanos@igtp.cat; 0000-0002-8133-5325

A.B.G.: abarrallo@ub.edu; 0000-0003-2086-8926

J.L.: jllorens@ub.edu; 0000-0002-3894-9401

Acknowledgements

This study was supported by grant number RTI2018-096452-B-I00 and PID2021-124678OB-I00 (Ministerio de Ciencia e Innovación, Agencia Estatal de Investigación, MCIU/AEI, 10.13039/501100011033, and European Regional Development Fund, FEDER), grant number 2017SGR621 (Agència de Gestió d'Ajuts Universitaris i de Recerca, AGAUR, Generalitat de Catalunya), and grant number 202007-30-31 (Fundació La Marató de TV3 2019) . A.B.G is a Serra-Húnter fellow. The electron and confocal microscopy studies were performed at the Centres Científics i Tecnològics de la UB (CCiTUB) of the Universitat de Barcelona. We thank Benjamín Torrejon-Escribano, Rosa Rivera, Adriana Martínez Gené, Mora Gimeno, Josep Manel Rebled and Eva Prats for the expert and technical help. We also thank Dr Bechara Kachar for the generous gift of the KCNQ4 antibody, and Dr. Erin A. Greguske for revision of the manuscript.

Competing interests

The authors declare no competing interests

ABSTRACT

Hair cell (HC) loss by epithelial extrusion has been described to occur in the rodent vestibular system during chronic 3,3'-iminodipropionitrile (IDPN) ototoxicity. This is preceded by dismantlement of the calyceal junction in the contact between type I HC (HCI) and calyx afferent terminals. Here, we evaluated whether these phenomena have wider significance. First, we studied rats receiving streptomycin for 3 to 8 weeks. Streptomycin caused loss of vestibular function associated with partial loss of HCI and decreased expression of CASPR1 (denoting calyceal junction dismantlement) in the calyces encasing the surviving HCI. Additional molecular and ultrastructural data supported the conclusion that HC-calyx detachment precede HCI loss by extrusion. Animals allowed to survive after the treatment showed functional recovery and rebuilding of the calyceal junction. Second, we evaluated human sensory epithelia obtained during therapeutic labyrinthectomies and trans-labyrinthine tumour excisions. Some samples showed abnormal CASPR1 label strongly suggestive of calyceal junction dismantlement. Therefore, reversible dismantlement of the vestibular calyceal junction may be a common response triggered by chronic stress before HCI loss. This may partly explain clinical observations of reversion in function loss.

54 **INTRODUCTION**

55 Sensory encoding by the inner ear's vestibular system depends on the transducing function of hair cells (HC). In
56 most mammals, permanent loss of equilibrium and gaze control occurs as a result of HC loss considering that
57 these cells do not regenerate to a significant extent to restore functionality. Nevertheless, significant recovery in
58 vestibular function is recorded clinically in a variety of disease conditions. In some cases, such as benign
59 paroxysmal positional vertigo (von Brevern et al., 2015), recovery can be complete, suggesting that the
60 condition is associated with pathogenic mechanisms that transiently impair the system's function, but do not
61 cause HC loss. In other disease conditions, such as Ménière's disease (López-Escámez et al., 2015), recurrent
62 crises are often associated with incomplete recovery and progressive worsening of the vestibular function. In
63 the case of exposure to ototoxic aminoglycoside antibiotics, irreversible loss of vestibular function is a common
64 outcome (Black et al., 2004), but significant yet incomplete recovery has also been recorded (Black et al., 2001).
65 In recent years, we have used a sub-chronic ototoxicity model to identify reversible cellular and molecular
66 alterations in the vestibular epithelia that associate with reversible loss of vestibular function in rats (Sedó-
67 Cabezón et al., 2015) and mice (Greguske et al., 2019). These studies showed that the sub-chronic ototoxic
68 stress caused by the experimental compound 3,3'-iminodipropionitrile (IDPN) results in the dismantlement of
69 the calyceal junction between type I HCs (HCI) and the calyx afferent terminals, as demonstrated by
70 ultrastructural characterization and observed loss of the junction proteins CASPR1 (contactin-associated protein)
71 and tenascin-C, as well as delocalization of the voltage-gated potassium channel KCNQ4. Simultaneously, the
72 vestibular epithelium showed a loss of pre-synaptic and post-synaptic proteins, indicative of synaptic uncoupling
73 between the HCs and their afferents. These changes that are associated with the loss of vestibular function are
74 revealed by visible behavioural deficits. In this model, if the exposure was halted at an early stage of the toxicity,
75 both the epithelium alterations and the behavioural dysfunction were largely reversible. In contrast, if the
76 exposure was maintained, the functional loss persisted as a result of HC loss, which predominantly occurred by

77 the extrusion of live cells from the sensory epithelium into the endolymphatic cavity (Llorens and Rodríguez-
78 Farré, 1997; Seoane et al., 2001a,b; Sedó-Cabezón et al., 2015; Greguske et al., 2019).

79 The rat and mouse sub-chronic IDPN models illustrate a cellular pathway to HC demise that differs from
80 apoptosis (Seoane et al., 2001a). As explained in the previous paragraph, it concludes with the extrusion of HCs
81 after a phase of sensory cell detachment and synaptic uncoupling (Sedó-Cabezón et al., 2015; Greguske et al.,
82 2019). The fact that extrusion is the main form of HC demise in birds and amphibians following a variety of
83 insults (Hirose et al., 1999; Rubel et al., 2013), suggests that its molecular mechanisms may be highly conserved
84 across vertebrates and operate in response to diverse forms of damage. Surprisingly, this phenomenon has
85 received scarce attention and information is lacking about its molecular mechanisms and relevance to human
86 health. One first question worth addressing is whether these phenomena have a role in mammalian
87 aminoglycoside toxicity *in vivo*, as this is the main cause of vestibular toxicity in humans. Although most research
88 on aminoglycoside-induced HC loss has focused on apoptosis (Furness, 2015), the literature also contains
89 evidence that these drugs may cause vestibular HC extrusion (Li et al., 1995; Nakagawa et al., 1997; Granados
90 and Meza, 2005). In the present work, we studied whether dismantlement of the calyceal junction, synaptic
91 uncoupling, and HC extrusion occur in the rat vestibular epithelium in response to one aminoglycoside
92 antibiotic, streptomycin. Previously, we found that the mode of HC demise, whether extrusion, apoptosis, or
93 necrosis was determined by the intensity and duration of the toxic stress. Thus, high acute doses of IDPN caused
94 HC necrosis, sub-acute exposure to medium doses caused HC apoptosis and sub-chronic low dose exposure
95 elicited HC extrusion (Seoane et al., 2001a). These data indicate that short exposure paradigms aimed at
96 accelerating and synchronizing HC demise (Taylor et al., 2008; Oesterle et al., 2008; Benkafadar et al., 2021) may
97 in fact favour the apoptotic pathways above other possible pathways. Accordingly, for the present study we
98 investigated the effects of sub-chronic aminoglycoside exposure. As a second approach to evaluate the
99 relevance of these phenomena to human disease conditions, we explored their occurrence in the vestibular
100 epithelia of a substantial number of patients with vestibular schwannoma and a few with other vestibular

101 diseases that also require trans-labyrinthine tumour excision (meningioma and endolymphatic sac tumour) or
102 therapeutic labyrinthectomy (Ménière's disease). Vestibular schwannomas are tumours that grow in the
103 vestibular nerve and cause hearing and vestibular function loss. Current evidence indicates that this loss may in
104 part be caused by the negative impact pro-inflammatory factors secreted by the tumour have on the sensory
105 epithelia (Dilwali et al., 2015). The data we obtained demonstrate that calyceal junction dismantlement occurs
106 during chronic streptomycin toxicity in rats and provide evidence that it occurs in human vestibular epithelia in
107 response to other types of stress.

108 **RESULTS**

109 **Effects of streptomycin sulphate on body weight and overall health.**

110 To study the sub-chronic toxicity of streptomycin on the vestibular system, we administered male and female
111 rats with one daily dose of streptomycin sulphate (0, 100, 300, 400 or 500 mg/kg x day - groups CTRL, STR-100,
112 STR-300, STR-400, STR-500) for up to 6 or 8 weeks, starting at day 21 of age. Other groups of rats were
113 administered with two daily doses of 0, 300, 350 or 400 mg/kg - groups CTRL, STR-300x2, STR-350x2, STR-
114 400x2). Rats administered with streptomycin showed an acute sedative effect starting within a few minutes
115 after each daily dose, and was most evident in the group receiving the highest dose (STR-500): the animal stayed
116 quiet with decreased responsiveness and with an overtly low muscle tone. This effect usually lasted 15-20 min
117 but sometimes lasted for up to two hours after injection. During this sedation period, two rats died in the STR-
118 500 group on days 5 and 36, likely from respiratory arrest. Additionally, two rats died for unknown reasons after
119 days 20 and 37 in the STR-300 and STR-500 groups, respectively. No animals died when larger daily doses were
120 administered via two daily injections. Recovery from this sedative effect was complete and surviving animals
121 showed normal behaviour except in regards to the evidences of vestibular dysfunction explained below. As
122 shown in Suppl. Fig. S1, streptomycin animals showed an increase in body weight at a smaller rate than that
123 shown by control rats. This resulted in significant differences in streptomycin versus control body weights after
124 five or more weeks of one daily dose, and by two weeks in the groups receiving two daily doses.

125 **Loss and recovery of vestibular function after sub-chronic streptomycin exposure.**

126 Sub-chronic exposure to streptomycin sulphate caused a dose-dependent loss of vestibular function, as
127 indicated by the rat's abnormalities in spontaneous motor behaviour. Vestibular deficient animals showed
128 ataxia, spontaneous circling, and head bobbing. The loss of function was assessed using high-speed video
129 records of the tail-lift reflex as described (Martins-Lopes et al., 2019; Maroto et al., 2021a,c). A similar dose-
130 dependent effect occurred in male and female animals (Suppl. Fig. S2), and therefore animals of both sexes

131 were pooled for all further analyses. The decrease in tail-lift angles, indicative of loss of vestibular function, was
132 not significant in the STR-100 group, and smaller in the STR-300 and STR-400 groups compared to the STR-500
133 group (Suppl. Fig. S3), so further analysis on the one daily dose paradigm focused on this dose level. As shown in
134 Figure 1A, a progressive reduction in tail-lift angles was recorded in the STR-500 rats. Repeated-measures
135 MANOVA of the tail-lift data from days 0 (pre-test) to 42 resulted in significant day ($F[6,28]=15.38$, $p<0.001$),
136 treatment ($F[1,33]=18.0$, $p<0.001$), and day X treatment interaction ($F[6,28]=9.766$, $p<0.001$) effects, with
137 significant differences between CTRL and STR-500 mean values recorded at 4 to 6 weeks of exposure. Extension
138 of the administration up to 8 weeks caused only a modest additional effect on vestibular function (Suppl. Fig.
139 S4A).

140 By administering streptomycin in two daily injections, larger doses could be given to the animals and circumvent
141 the risk of death associated with the acute sedative effects of the drug. As shown in Fig. 1B, all the STR-300x2,
142 STR-350x2, and STR-400x2 groups showed faster and deeper loss of vestibular function than the STR-500 group.
143 MANOVA of the tail-lift data from the two daily injections experiment up to day 21 resulted in significant day
144 ($F[3,26]=191.1$, $p<0.001$), treatment ($F[3,28]=45.89$, $p<0.001$), and day X treatment interaction ($F[9,63.4]=20.92$,
145 $p<0.001$) effects. The effect was dose-dependent, and larger doses caused a faster progression of the decline in
146 vestibular function.

147 To evaluate the potential for functional recovery, some animals were allowed to survive after the end of the
148 sub-chronic streptomycin exposure. As shown in Fig. 1C, rats exposed to 500 mg/kg · day of streptomycin for 6
149 weeks recovered normal tail-lift angles during the washout period. Functional recovery was also observed in the
150 STR-500 rats exposed for 8 weeks (Suppl. Fig. S4B). The individual values of animals allowed to recover after 3
151 weeks of two daily doses of streptomycin also showed a clear recuperation of the tail-lift reflex (Fig. 1D).

152 **Sub-chronic streptomycin exposure caused partial loss of HCs in the vestibular sensory epithelia.**

153 To evaluate the major effects of streptomycin on the vestibule, we observed surface preparations of the sensory
154 epithelia using scanning electron microscopy (SEM). As reported in previous studies (Llorens et al., 1993; Seoane
155 et al., 2001a; Sedó-Cabezón et al., 2015), SEM observation of control epithelia (n=16) (Fig. 2A; Suppl. Fig. S5A, B)
156 revealed morphological features matching literature descriptions of healthy untreated rats with high densities of
157 stereocilia bundles. Epithelia from STR-300 animals (6 weeks of exposure, n=3) showed similar features to
158 control epithelia, except for indications of a few missing hair bundles or occasional bundles with fused
159 stereocilia (data not shown). For animals administered with larger doses of streptomycin once a day, the SEM
160 observations revealed scant to moderate loss of stereocilia bundles. Similar findings were obtained in STR-500
161 rats with small difference observed between animals exposed for 6 (n=6) or 8 (n=7) weeks, and in STR-400 rats
162 exposed for 8 weeks (n=2). Hair bundle loss was roughly similar in cristae (Suppl. Fig. S5C), utricles (Suppl. Fig.
163 S5D), and saccules (Fig 2B, C), with no evidence of an overt difference in susceptibility among receptors. In all
164 cases, the loss of stereocilia bundles was partial and many bundles were still present in the sensory receptors of
165 the worst cases (Suppl. Fig. S5E,F). In these SEM observations, images indicating ongoing damage were scarce.
166 Nevertheless, some evidence for fused stereocilia and HC protrusion were found (Fig 2D,E). Animals given two
167 daily injections of streptomycin displayed a larger loss of stereocilia bundles than the animals administered for
168 once a day (Suppl. Fig. S6). Evidence for ongoing damage was scarce in some epithelia, but clear in other
169 samples, including images of epithelial scars, bundle fusion, and cell protrusion towards the endolymphatic
170 cavity (Suppl. Fig. S6). The average extent of hair bundle loss was similar in STR-300x2 rats treated for 6 weeks
171 (n=7), STR-350x2 rats treated for 4 weeks (n=6), and STR-400x2 rats treated for 3 weeks (n=6).

172 To determine the loss of HCs revealed by the decreased densities of hair bundles observed by SEM in STR-500
173 rats, we obtained type I HC (HCI) and type II HC (HCII) counts from the vestibular epithelia of the other ear of the
174 same animals. To this end, we immunostained the epithelia with antibodies against myosin-7a (MYO7A),
175 CASPR1, and the calcium-binding protein calretinin, revealed by fluorescent secondary antibodies. In the
176 confocal microscopy images, HCI were identified as MYO7A+ cells (a pan-HC marker, Hasson et al., 1997)

177 surrounded by a CASPR1+ calyx (Sousa et al., 2009; Lysakowski et al., 2011; Sedó-Cabezón et al., 2015), even if
178 weak or fragmented, or with an unambiguous HCI shape with a long and narrow neck. As an estimate of HCII, we
179 counted cells with double MYO7A and calretinin label (Dechesne et al., 1991). The data obtained, presented in
180 Fig. 3A-C, reveal a significant decrease in HCI counts in both peripheral and central/striola regions of the crista
181 and the utricle and in the periphery of the saccule. ANOVA results were: central crista, $F[3,27]= 12.82$, $p<0.001$;
182 peripheral crista, $F[3,24]=2.89$, $p=0.056$; central utricle, $F[3,25]=23.86$, $p<0.001$; peripheral utricle,
183 $F[3,26]=44.95$, $p<0.001$; central saccule, $F[3,20]=2.01$, $p=0.15$ - N.S.; peripheral saccule, $F[3,22]=8.31$, $p=0.001$.
184 The most affected receptor was the utricle with a 52-67 % decrease in HCI counts in STR-500 animals, followed
185 by the crista, where a 30-40 % loss was recorded. In both the crista and the utricle, similar effects were recorded
186 in animals exposed for 6 weeks and animals exposed for 8 weeks. In the saccule, the loss was smaller than in the
187 crista and utricle receptors, and greater at 8 weeks than at 6 weeks of treatment. HCI counts remained reduced
188 in animals allowed to recover after the end of the exposure period, indicating an insignificant capacity for
189 regeneration. In contrast to HCI, no significant differences were obtained among treatment groups in HCII
190 counts (all p values > 0.1).

191 As explained above, the SEM observations indicated a loss of HC after two daily injections of streptomycin
192 greater than that recorded after one daily injection. To estimate HC loss according to cell type, we
193 immunostained crista receptors with antibodies against secreted phosphoprotein 1 (SPP1) / osteopontin,
194 CASPR1, and calretinin. HCI were identified by the SPP1 label (Burns et al., 2015; McInturff et al., 2018; Maroto
195 et al., 2021b), while the main population of HCII was identified by the calretinin+ label. As shown in Fig. 3D,E,
196 the number of HCI was greatly reduced after two daily injections of streptomycin ($F[4,26]=84.6$; $p<0.001$), while
197 the number of HCII was unchanged ($F[4,26]=1.45$, $p=0.25$). The loss of HCI was similar in the three groups of rats
198 treated with streptomycin (STR-300x2, STR-350x2, STR-400x2), and no recovery in HCI counts was recorded in
199 the washout group.

200 **Calyceal junction dismantlement, afferent fragmentation, and synaptic loss after sub-chronic streptomycin**
201 **exposure.**

202 In addition to HCl loss, rats exposed to sub-chronic streptomycin displayed alterations in the remaining HCIs and
203 their afferents. In rats exposed to streptomycin once a day (STR-500), a reversible loss of CASPR1 fluorescence
204 occurred in the calyces contacting the surviving HCIs (Fig.5). To assess this effect, we measured the amount of
205 CASPR1 fluorescence associated with the remaining individual calyces. The loss and recovery of the CASPR1 label
206 was found across the three epithelia and in both central/striolar and peripheral zones. All ANOVA comparisons
207 resulted in significant differences (all $F[3, 19 \text{ to } 27] > 5.3$, all $p's<0.006$). As shown in Fig. 4, the confocal
208 microscope images also revealed a reversible decrease in MYO7A fluorescence intensity in the HCs of the STR-
209 500 animals. This effect was quantified in a subset of samples and significant group differences were found
210 ($F[2,11]=5.0$, $p=0.029$). The post-hoc analysis confirmed that the label (in arbitrary units) was reduced from 9583
211 $\pm$ 1290 ($X\pm SE$, n=5) in CTRL animals to 6232 $\pm$ 781 (n=4) in STR-500 (8 wk) animals ($p<0.05$, Duncan's test), and
212 recovered (10522 $\pm$ 621, n=5) after washout. In animals given two injections a day, the intensity of CASPR1
213 immunoreactivity in the calyces contacting surviving HCI was also reduced by streptomycin (Suppl. Fig. S7).

214 We also evaluated whether sub-chronic streptomycin altered the distribution of the potassium channel, KCNQ4,
215 in the calyx membrane, as identified in CASP1-KO mice (Sousa et al., 2009) and in rats exposed to sub-chronic
216 IDPN (Sedó-Cabezón et al., 2015). The data, shown in Fig. 5A,B, indicated that CASPR1 loss is associated with
217 KCNQ4 redistribution in the calyces of the STR-500 rats. In control rats, the KCNQ4 label is found almost
218 exclusively in the inner membrane, that is, in the calyceal junction area, and is absent in the outer membrane of
219 the calyx. After streptomycin treatment, the immunofluorescence was reduced in the inner membrane, whereas
220 significant labelling appeared in the outer membrane of the calyx. Therefore, KCNQ4 was abnormally distributed
221 after streptomycin. ANOVA analyses of the amount of fluorescence in the inner and outer membranes were
222 significant ($F[3, 14]=12.1$, $P<0.001$, and $F[3,14]=49.9$, $p<0.001$, respectively). Post-hoc analyses confirmed that
223 streptomycin caused KCNQ4 redistribution, and that this effect was no longer present in the washout animals.

224 Sub-chronic streptomycin also caused a reduction in the number of synaptic puncta as revealed by labelling with
225 antibodies against ribeye/CtBP2, the core protein of the presynaptic ribbon, and against the post-synaptic
226 scaffold protein PSD-95 (post-synaptic density 95). The mean number of puncta counts per cell in 2.7 μm thick
227 sections of HCs was significantly reduced in STR-500 animals exposed for 6 weeks compared to CTRL animals
228 (Fig. 5C,D). T-test comparisons resulted in $p < 0.001$, $p=0.018$, and $p=0.001$ for ribeye, PSD-95, and co-localization
229 values, respectively.

230 The effect of sub-chronic streptomycin on the calyceal junction was also studied at the ultrastructural level by
231 TEM observation of samples from control rats (4 lateral crista, 2 saccules, 1 utricle), STR-500 rats exposed for 6
232 (5 lateral crista) or 8 (4 lateral crista) weeks, and STR-300x2 rats exposed for 6 weeks (3 saccules and 1 utricle).
233 In control specimens, calyceal junctions were prominent with virtually no disruptions in the two basal thirds of
234 contact between HCI and its afferent calyx (Fig. 6A,C). This junction consists of highly electron-dense pre- and
235 post-synaptic membranes, a highly regular inter-membrane distance, and an electron-dense extracellular space.
236 In contrast, many calyces in the streptomycin rats showed from fragmented to only partial to absent junctions
237 (Fig. 6B, D-F). In these units, the membrane density was similar to that of regular membranes and the area
238 displayed a more-variable inter-membrane distance, as well as a reduced extracellular electron density. In
239 addition, fragmented calyces were also identified in the samples from the treated animals, and these showed
240 absence of the calyceal junction (Fig. 6E, F). No fragmented calyces were observed in the control epithelia.

241 **Hair cell extrusion after sub-chronic streptomycin exposure.**

242 The occurrence of HC extrusion was evaluated by immunofluorescent analysis in samples from animals exposed
243 to streptomycin twice a day. The MYO7A and CASPR1 antibodies were combined with an anti-radixin antibody to
244 label the apical microvilli of the supporting cells and thus outline the surface of the epithelium. Images indicating
245 HC extrusion were not obtained in most sections of the crista (n=4 CTRL, 7 STR-300x2, 4 STR-350x2, and 4 STR-
246 400x2) and saccule (n=2 CTRL, 7 STR-300x2, 5 STR-350x2, and 6 STR-400x2). However, as illustrated in Fig. 7A,

247 protruding/extruding HCs were a common finding in most utricle sections from animals exposed to STR-300x2
248 for 6 weeks (n=7) or STR-350x2 for 4 weeks (n=5), although not in utricles from animals receiving STR-400x2 for
249 3 weeks (n=6). Control utricles (n=2) also showed no HC extrusion. In the STR-300x2 and STR-350x2 utricles, the
250 occurrence was around 1-3 protruding/extruding HC per section (130-190 μm long, 25 μm thick).

251 To corroborate that the extruding MYO7A+ profiles found in the immunofluorescent analyses corresponded to
252 living HCs, we examined two utricles by TEM. As shown in Fig. 7B,C, the extruding HC showed displacement of
253 the whole cell towards the lumen of the utricle. The ultrastructural features of the cytoplasm, organelles, and
254 nucleus indicated continued activity of the cell.

255 **Occurrence of calyceal junction dismantlement in human vestibular epithelia.**

256 To evaluate whether calyceal junction dismantlement also occurs in human vestibular epithelia under stress, we
257 studied samples from patients submitted to therapeutic labyrinthectomy or translabyrinthine tumour excision.
258 The vestibular epithelia were immunolabeled with anti-CASPR1 antibodies combined with a variety of other
259 antibodies, and a total of 29 samples yielded useful information. MYO7A, calretinin, and CASPR1 labels matched
260 the labelling features described above in rat samples. Also, when tested together (n=9), CASPR1 and the
261 extracellular matrix protein tenascin-C were found to localise together in the calyceal junction area, as described
262 previously in rodent samples (Lysakowski et al., 2011; Sedó-Cabezón et al., 2015; Greguske et al., 2019). In
263 contrast, the observed label of HCI by SPP1 was unreliable in the tested conditions. Among the 29 epithelia, HC
264 densities varied from high, similar to that observed in samples from control rats, to almost null. Reduced HC
265 density could result from both the patient's age and vestibular pathology; the evaluation of this pathology was
266 beyond the scope of the present study. Regarding the calyceal junctions, 18 samples were evaluated to have
267 intact or mostly intact CASPR1-labelled calyces. These included 2/2 cases of Ménière's Disease (Fig. 8A), 4/4
268 cases of meningioma (Fig. 8B,C), 1/1 case of an endolymphatic sac tumour, and 11/22 cases of vestibular
269 schwannoma. Two other samples displayed very few HCs with only one CASPR1+ or none, hampering the

270 achievement of any conclusion on calyceal junctions. However, 9 of the samples, all of them from vestibular
271 schwannoma patients, provided images suggesting that an active process of calyceal junction dismantlement
272 was taking place. This included calyces with patched CASPR1 labelling (Fig 8D-F) or lack of CASPR1 in calyx-only
273 units (Fig. 8G). The patched feature of the label in some calyces was confirmed in 3D reconstructions (Suppl. Fig.
274 S8). The number of days the samples were in fixative does not explain this effect, as it was observed in tissues
275 fixed for 1 day (n=5), 4 days (n=1), 7 days (n=1), and unrecorded (but less than 8) days (n=2).

276 **DISCUSSION**

277 Previous work from our laboratory in rats and mice has demonstrated that sub-chronic IDPN exposure causes
278 vestibular HC extrusion and that the extrusion is preceded by reversible calyceal junction dismantlement and
279 synaptic uncoupling (Seoane et al., 2001a; Sedó-Cabezón et al., 2015; Greguske et al., 2019). These phenomena
280 have received little research attention despite its potential relevance. HC extrusion is the main form of HC
281 demise in birds and amphibians (Hirose et al., 1999; Rubel et al., 2013) and has been sporadically observed in
282 mammalian vestibular epithelia (Li et al., 1995; Nakagawa et al., 1997; Granados and Meza, 2005). In the present
283 work, we first aimed at establishing a new rat model of sub-chronic aminoglycoside toxicity to determine
284 whether HC detachment and extrusion occur in ototoxic conditions of clinical relevance. The data obtained
285 demonstrate that the calyceal junction reversibly dismantles during subchronic streptomycin exposure in
286 association with reversible vestibular dysfunction. Synaptic uncoupling and HC extrusion were also recorded in
287 these rats. In addition, we also collected evidence indicating that calyceal junction dismantlement may take
288 place in the human vestibular system.

289 HC degeneration is effectively achieved by direct exposure to aminoglycoside antibiotics as done by trans-
290 tympanic administration or in *in vitro* studies (Kohonen and Tarkkanen, 1969; Anniko et al., 1982). However, the
291 use of more natural *in vivo* approaches to induce inner ear toxicity in laboratory animals with aminoglycosides
292 has been a challenging issue, as acute systemic intoxication may not cause ototoxic effects until the dose is large
293 enough to trigger animal death (Wu et al., 2001; Murillo-Cuesta et al., 2010). Nevertheless, several studies have
294 succeeded in establishing dosing regimes that elicit ototoxic effects with limited lethality and systemic toxicity.
295 Yet, many of these studies favour cochlear versus vestibular toxicity (Sullivan et al., 1987) or are designed to
296 accelerate the progression of the damage (Taylor et al., 2008; Oesterle et al., 2008). In the present study, we
297 successfully caused slowly progressing vestibular toxicity with streptomycin in young rats. By means of one daily
298 injection, significant loss of vestibular function occurred after four weeks of the highest tolerated dose, while
299 the use of two injections per day accelerated this loss in a dose-dependent manner, allowing for the study of

300 ototoxicity emerging after 2-3 weeks of treatment. Interestingly, the effects were similar in both sexes and low
301 variability was recorded within groups. Thus, as similarly reported for cochlear kanamycin toxicity in rats and
302 mice (Wu et al., 2001; Jiang et al., 2006), exposure of Long-Evans rats to one or two daily doses of streptomycin
303 reliably causes vestibular toxicity. Comparing the two models, it appears that the one daily dose regimen
304 reaches a limit in its effect, while the two-dose regimen seems to provide a more flexible model to study dose-
305 and time-dependent effects.

306 Streptomycin exposure in rats caused the loss of HCs, deeper after two daily doses than after one dose, as
307 revealed by the SEM studies and quantified in immunofluorescence studies. Separate counts of HCI and HCII
308 revealed that HC loss concentrated on the HCI, while HCII were spared in both injection paradigms. To identify
309 HCI we used two different markers, CASPR1 and SPP1. CASPR1 is not expressed by HCIs but is found in the
310 membrane of the calyx afferent contacting the HCI (Sousa et al., 2009; Lysakowski et al., 2011; Sedó-Cabezón et
311 al., 2015). Although streptomycin caused a specific loss of CASPR1, traces of CASPR1 label in contact with cell
312 profiles positive for Myo7a+ and negative for calretinin (see Fig 3A) allowed a reliable identification of HCI in the
313 one dose samples. Also, except for a minor recovery in HCI numbers in the periphery of utricles and cristae, no
314 increase in HCI numbers was found in the samples of the washout animals, in which a good recovery in CASPR1
315 expression had occurred. In addition, the loss of HCI was confirmed using a positive HCI marker, SPP1 (McInturff
316 et al., 2018), to evaluate the samples from the two daily injections experiment. To identify HCII, we also used a
317 positive marker, calretinin, and found that the number of HCII per image was not reduced in any of the two
318 exposure paradigms. Because of the method used, we cannot completely exclude that a small loss of HCII was
319 masked by tissue shrinkage, but in any case the lack of differences in HCII numbers per image contrasts with the
320 significant loss of HCI. While a greater sensitivity of HCI with respect to HCII in regards to ototoxic insult is widely
321 recognized, not many studies are available in providing a quantitative assessment of this difference *in vivo*
322 (Lopez et al., 1997; Nakayama et al., 1996 ; Hirvonen et al., 2005; Maroto et al., 2021a).

323 The data collected add to the existing evidence that HC extrusion is a significant form of HC demise induced by
324 aminoglycosides in the mammalian vestibular system *in vivo*, as reported in the vestibular epithelia of rodents
325 exposed to other aminoglycosides using relatively long exposure paradigms (Li et al., 1995; Granados and Meza,
326 2005). Also, the present data demonstrate that calyceal junction dismantlement and synaptic uncoupling occur
327 after streptomycin, as previously demonstrated for sub-chronic IDPN (Sedó-Cabezón et al., 2015; Greguske et
328 al., 2019). The streptomycin effect includes CASPR1 down-regulation, redistribution of KCNQ4, loss of electron
329 density in the calyceal junction area, and a reduction in the number of synaptic puncta per cell. As observed in
330 the IDPN model, these effects are associated with the loss of vestibular function, and significant recovery was
331 also recorded for the behavioural, CASPR1, and KCNQ4 effects in rats when allowed a washout period after the
332 exposure. However, significant differences between the two models were noticed. In the rat IDPN model
333 (Seoane et al., 2001a; Sedó-Cabezón et al., 2015), a complete dismantlement of the calyceal junctions, with
334 extensive loss of CASPR1 and redistribution of KCNQ4 occurs before HC loss starts. Extending the time of IDPN
335 exposure triggers a massive event of HC extrusion, and the occurrence of extruding cells over several weeks
336 indicates that the extrusion of each HC takes place over several days. IDPN thus provides a highly synchronic and
337 slowly progressing model of sequential HC detachment and extrusion. In contrast, in the streptomycin rats,
338 extruding HC were only found occasionally, the loss of CASPR1 and the redistribution of KCNQ4 were smaller,
339 and a significant loss of HCs had occurred already before complete dismantlement of the calyceal junctions.
340 These observations indicate that, in comparison to those of IDPN, the effects of streptomycin are less
341 synchronic, and that the extrusion of each HC takes place in a shorter time, probably a few hours. Although not
342 specifically addressed in the present experiments, the TEM studies did not give evidence for an extensive
343 occurrence of apoptotic HC death. The simplest explanation of the present observations is that HC detachment
344 and extrusion are triggered at the individual cell level, and that cells are not synchronized after streptomycin
345 treatment as they are after IDPN. This conclusion is supported by our previous demonstration that calyceal

346 junction dismantlement is triggered individually in a calyx-to-calyx basis also after IDPN (Sedó-Cabezón et al.,
347 2015).

348 Behavioural and CASPR1 data presented here demonstrate repair capacity and functional recovery of the rat
349 vestibular epithelium after sub-chronic streptomycin exposure. Although only a limited number of animals were
350 allowed to survive, their recovery was indubitable. Functional recovery may be a consequence of behavioural
351 compensation or reflect recovery from alterations not detected by histological analyses, such as hypothetical
352 changes in endolymph composition or inactivation of the transduction channels. Conversely, our data excluded
353 the possibility that HC regeneration accounted for this recovery, because HCI counts remained decreased at the
354 end of the washout period. Rather, its association with the reversal in CASPR1 labelling, as measured on a cell-
355 by-cell basis, suggests that the functional recovery may result, at least in part, from repair phenomena in the HC
356 and the contact between HCs and their afferents. The present observation of a recovery in CASPR1 labelling
357 contradicts the persistence of calyceal pathology observed in chinchillas exposed to gentamicin by direct
358 perilymphatic infusion (Sultemeier and Hoffman, 2017). Differences in species, aminoglycosides, and exposure
359 model may account for the difference between the present data and those by Sultemeier and Hoffman (2017).

360 To explore the possible relevance of the calyceal junction dismantlement to human pathology, we examined a
361 series of human samples for histological evidence of such dismantlement. The interpretation of the human
362 observations is weakened by the lack of control samples, and the variability in pathological conditions and
363 surgery-generated damages. Nevertheless, many samples included a uniform CASPR1 label in all observable
364 calyces, while some other samples offered multiple images of patched or largely missing label for this protein.
365 Although the possibility that this abnormality was generated during collection of the sample cannot be
366 completely excluded, the data strongly suggest that calyceal junction dismantlement may indeed occur in the
367 human vestibule under stressful conditions. Although all the cases in which CASPR1 loss was recorded were
368 from vestibular schwannoma surgeries, the number of samples from other pathologies was so low that it cannot
369 be discarded that similar observations could emerge if more cases were examined. Current evidence indicates

370 that vestibular schwannomas may damage the sensory epithelia of the inner ear through tumour-secreted
371 factors, including tumour necrosis factor alpha (TNFα) (Dilwali et al., 2015). A recent study has demonstrated
372 the potential of this pro-inflammatory cytokine to cause cochlear synaptic uncoupling *in vivo* (Katsumi et al.,
373 2020). It is thus possible that inflammatory signals like TNFα are able to trigger the dismantlement of the
374 calyceal junction, synaptic uncoupling, and eventual HC extrusion in the vestibular epithelium.

375 Future work may address some of the limitations of this initiating study and use it to expand our understanding
376 of vestibular pathophysiology. For instance, determining the blood and inner ear concentrations of streptomycin
377 (and its potential ototoxic metabolites, e.g. Granados and Meza, 2005) in this exposure model may enlighten the
378 role of inner ear accumulation in systemic aminoglycoside toxicity. Recent data supports that cochlear retention
379 is a key factor in cisplatin ototoxicity (Breglio et al., 2017), and some data is available supporting a similar
380 conclusion for the cochlear and vestibular toxicity of gentamicin (Imamura and Adams, 2003). More works is
381 also needed to replicate and expand the human observations, excluding any potential confounding factor and
382 relating the pathological findings to the clinical data of patients. This is particularly important due to the lack of
383 tissues from humans not suffering any inner ear disease.

384 In conclusion, the present study evaluated whether events leading to HC extrusion in the vestibular sensory
385 epithelia of rodents exposed to sub-chronic IDPN (Seoane et al., 2001a; Sedó-Cabezón et al., 2015; Greguske et
386 al., 2019) may have a wider significance. The data collected demonstrate that dismantlement of the calyceal
387 junction and synaptic uncoupling are widespread phenomena in rats exposed to sub-chronic streptomycin
388 regimes that cause HC loss through, at least in part, the extrusion pathway. We also collected data suggesting
389 that calyceal junction dismantlement may occur in human vestibular epithelia in response to inflammatory
390 stress. Elucidating the molecular pathways triggering these cellular phenomena may unveil new targets to
391 control damage progression in this sensory epithelium.

392 **MATERIALS AND METHODS**

393 **Animals and treatments**

394 Animals were used in accordance with Law 5/1995 and Act 214/1997 of the Generalitat de Catalunya and
395 approved by the University of Barcelona's Ethics Committee on Animal Experiments and the Commission on
396 Animal Experimentation of the Generalitat. Long-Evans rats were obtained from Janvier Labs (Le-Genest-Saint-
397 Isle, France) at post-natal day 8-12. They were housed with lactating mothers in standard Macrolon cages
398 (215×465×145 mm) with wood shavings as bedding. At day 21, the rats were weaned and housed in groups of
399 four of the same sex. Housing conditions included a 12:12 h light:dark cycle (07:30-19:30 h), a 22±2°C room
400 temperature and an *ad libitum* access to standard pellet diets (TEKLAD 2014, Harlan Laboratories, Sant Feliu de
401 Codines, Spain).

402 A total of 98 rats (58 males, 40 females) were used in two different administration protocols, one injection per
403 day and two injections per day. The first administration protocol was designed on the grounds of the protocols
404 by Granados and Meza, 2005, and Schirmer et al., 2007. Animals were administered streptomycin sulphate salt
405 (Sigma-Aldrich, S6501), s.c., dissolved in PBS, starting at postnatal 21, daily for 6 or 8 weeks. To ensure dose
406 accuracy, injection volumes were 10 ml/kg at the beginning, but were reduced to 2 ml/kg as the rats increased
407 body weights. Different injection sites in the dorsal skin were used in an alternating sequence. In this first series
408 of experiments, rats were dosed with 0 (control vehicle), 100, 300, 400 or 500 mg/kg · day of streptomycin
409 (referred to the free base), once a day, for 6 or 8 weeks. Two experimental batches used only males, one of
410 them used only females, and the fourth one included an equal number of males and females. Acute toxicity and
411 lethality is described in the results section above. A final experiment used a second administration protocol, in
412 which the total daily dose was split into two injections given 8 h apart. This dosing paradigm was designed to
413 evaluate the vestibular effects of larger daily doses and circumvent the acute toxicity of streptomycin recorded
414 in rats receiving the 500 mg/kg dose. Thus, rats received 0, 600, 700 or 800 mg/kg · day in two daily doses of 0,

415 300 mg/kg (for 6 weeks), 350 mg/kg (for 4 weeks) or 400 mg/kg (for 3 weeks). No animals died in this
416 experiment. The detail of all groups of animals used is shown in Supplementary Table S1.

417 During the period of treatment, the animals were weighted and assessed for wellbeing daily. They were also
418 tested for vestibular function once a week. At the end of the treatment period, some animals were allowed to
419 survive for up to 8-10 additional weeks to evaluate the potential reversibility of the vestibular dysfunction and
420 the histopathological effects of streptomycin. Some control animals were also allowed to survive the washout
421 period to provide control body weight and vestibular function data. The day after that of the last dose, or after
422 the washout period, rats were euthanized by decapitation under anaesthesia. The skull was sectioned in half and
423 placed in fixative solution under a fume hood for dissection of the vestibular sensory epithelia. The epithelia
424 from the first ear were typically obtained within 5 min after decapitation and used for scanning (SEM) and
425 transmission (TEM) electron microscopy. The epithelia from the second ear, obtained within 15 min after
426 decapitation, were used for immunohistochemistry. Epithelia from some animals were used for
427 immunohistochemical analysis only. The numbers of animals used in each histological analysis are indicated in
428 the figures and are summarized in Suppl. Table S2.

429 **Human samples**

430 Vestibular sensory epithelia were collected from patients submitted to therapeutic labyrinthectomy or
431 translabyrinthine tumour excision. The samples included in the study, detailed in Suppl. Table S3, are from 2
432 cases of Ménière's Disease, 1 case of endolymphatic sac tumour, 4 cases of meningioma, and 22 cases of
433 vestibular schwannoma. Patients were 18 to 70 years old, and 52 % were females. The tissues were obtained
434 after informed consent, as approved by the Clinical Ethics Committee of the Hospital Germans Trias i Pujol. The
435 samples were immediately placed in 4% formaldehyde with <2.5% methanol (BiopSafe) and sent to the
436 laboratory, usually in 24 h, although some samples were delayed for up to 7 days (Suppl. Table S3). The tissues

437 were then rinsed in phosphate buffered saline (PBS, pH 7.2), transferred into a cryoprotective solution (34.5%
438 glycerol, 30% ethylene glycol, 20% PBS, 15.5% distilled water) and stored at -20ºC until further processing.

439 **Assessment of vestibular function in rats**

440 To evaluate vestibular function, we assessed the tail-lift reflex as described (Martins-Lopes et al., 2019; Maroto
441 et al., 2021 a,c). Briefly, rats are held by the base of the tail and quickly but gently lifted upwards to
442 approximately 40 cm above ground and immediately returned down. In healthy rats, this triggers a trunk and
443 limbs extension reflex in a landing response. Loss of vestibular function results in loss of the anti-gravity
444 extension reflex, so the rat curls ventrally (Hunt et al., 1987; Pellis et al., 1991; Llorens et al., 1993; Maroto et al.,
445 2021c). The reflex response of the animal is recorded from the side with high-speed video (we use 240 frames
446 per second with a GoPro 5 camera) and the records are used to obtain the minimum angle formed by the nose,
447 the back of the neck and the base of the tail during the tail-lift manoeuvre (tail-lift angle, TLA), as described
448 (Martins-Lopes et al., 2019; Maroto et al., 2021a,c). The TLA has been demonstrated to provide an objective
449 measure of permanent or reversible vestibular loss (Martins-Lopes et al., 2019; Maroto et al., 2021a,c).

450 **Electron microscopy**

451 For SEM and TEM, rat vestibular epithelia were dissected in 2.5% glutaraldehyde in 0.1 M cacodylate buffer (pH
452 7.2), and fixed overnight in this solution. The epithelia were then rinsed with cacodylate buffer, post-fixed for 1
453 h in 1% osmium tetroxide in the same buffer, rinsed again and stored in 70% ethanol at 4ºC until further
454 processing. Afterwards, the samples were dehydrated with increasing concentrations of ethanol, up to 100%.
455 For TEM analysis, the lateral crista was embedded in Spurr resin. To select the level of interest, semi-thin
456 sections (1 µm) were stained with 1% toluidine blue and examined in a light microscope. Ultrathin sections were
457 stained with uranyl acetate and lead citrate and were observed with a JEOL 1010 microscope at 75-80 kV. For
458 SEM analysis of epithelial surfaces, the dehydrated specimens were dried in a Polaron E3000 critical-point dryer
459 using liquid CO2, coated with carbon, and observed in a JEOL JSM-7001F field emission SEM.

460 **Immunohistochemistry**

461 The following commercial primary antibodies were used: mouse monoclonal anti-CASPR1 (clone K65/35, RRID:
462 AB_2083496, used at 1:400 dilution) and anti-PSD95 (clone K28/43, RRID: AB_2292909, 1:100) from the UC
463 Davis / NIH NeuroMab Facility; mouse monoclonal anti-Ribeye/CtBP2 (clone 16/CtBP2, BD Transduction Labs,
464 RRID: AB_399431, 1:100); rabbit anti-myosin VIIa (25-6790, Proteus Biosciences, RRID: AB_10015251; 1:400);
465 guinea pig anti-calretinin (214.104, Synaptic Systems, RRID: AB_10635160, 1/500); goat anti-SPP1 (AF808, RD
466 systems, RRID: AB_2194992, 1/200). We also used a rabbit anti-KCNQ4 (PB-180, 1/1000) donated by Bechara
467 Kachar (National Institute on Deafness and Other Communication Disorders, NIH; Beisel et al., 2005). To reveal
468 the primary antibodies, we used Day-Light-405, Alex-488, Alexa-555 and Alexa-647-conjugated secondary
469 antibodies from Invitrogen / Thermo Fisher. To image synaptic puncta, we used isotype-specific secondary
470 antibodies, i.e., anti-mouse-IgG1 to reveal the Ribeye/CtBP2 antibody and anti-mouse IgG2a to reveal the PSD-
471 95 antibody.

472 After dissection, the rat vestibular epithelia were fixed for 1 h at room temperature in 4 % paraformaldehyde in
473 PBS. These samples were rinsed in PBS, transferred into the cryoprotective solution and stored at -20ºC. To
474 circumvent potential bias from batch-to-batch differences in immunolabelling, we processed in parallel
475 specimens from each experimental group. For immunolabelling, rat or human tissues were washed with PBS to
476 remove the cryoprotective solution, permeated in 4% Triton-X-100 in PBS for 1 h at room temperature, and then
477 blocked in 0.5% Triton-X-100 and 1% fish gelatine in PBS (Sigma-Aldrich, cat.# G7765) also for 1 h at room
478 temperature. They were then incubated with the mixed primary antibodies in 0.1% Triton-X-100 and 1% fish
479 gelatine in PBS for 24 h at 4ºC, followed by incubation with the secondary antibodies in the same conditions.
480 The samples were thoroughly rinsed with PBS following each incubation and gently rocked during the
481 incubations and washes. The immunolabelled human epithelia were whole-mounted in Mowiol medium,
482 whereas the rat epithelia were sectioned before mounting in the same medium. To obtain sections, the tissues
483 were embedded in a mixture of 0.49% gelatin, 30% bovine serum albumin, and 20% sucrose in PBS overnight at

484 4 ºC. This same medium was used to form a block by solidification with 2 % glutaraldehyde, one sample placed
485 oriented in its surface, and a second block formed on top of it. Using a Leica VT1000S vibrating microtome,
486 sections of 40 μm were obtained from this layered block with the specimen placed in between the two halves. A
487 detailed version of this protocol has been published (Maroto et al., 2021b).

488 **Confocal microscopy observation and analysis**

489 Tissue sections were observed in a Zeiss LSM880 spectral confocal microscope. In animal studies, image
490 acquisition settings were maintained across samples from each immunolabelling batch. To obtain HC counts, Z-
491 stacks of optical sections were obtained each 0.5 μm spanning 25 μm with the 63X objective. Then, we obtained
492 8 sequential images (3 μm thick each) by the maximum intensity projection of 6 consecutive images from the
493 original stack. The ImageJ software (National Institute of Mental Health, Bethesda, Maryland, USA) was used for
494 quantitative image analyses. Epithelia of animals injected once a day with streptomycin were labelled with anti-
495 MYO7A, anti-CASPR1, and anti-calretinin antibodies. HCI were defined as MYO7A+ cells surrounded by a calyceal
496 CASPR1+ label, even in cases where this label appeared thin and fragmented, or cells with an unambiguous HCI
497 shape with a long and narrow neck. HCII were defined as cells labelled with both the anti-MYO7A and anti-
498 calretinin antibodies. MYO7A+ cells not identified as HCI or HCII (3-6 %) were excluded from the analysis. For
499 each animal and epithelial zone, the number of HCI and HCII per image was obtained by averaging counts from
500 the 8 images of a representative histological section. The histological sections used for counting were obtained
501 from similar locations in all animals. To evaluate the loss of CASPR1 label in the calyces, the amount of
502 fluorescence in the corresponding colour channel was measures in individual calyces using a 100 μm^2 region of
503 interest on a single optical section. For each animal, epithelium and zone, the average amount of fluorescence
504 was obtained from all HCs available for analysis up to 40 cells. Data were normalized as percentage of the mean
505 fluorescent intensity of control samples in the same batch of immunohistochemical processing and confocal
506 imaging. Then, statistical analyses were performed to compare among groups of animals. To compare the

507 distribution of KCNQ4 in the inner and outer membranes of the calyx, we assessed the profile of fluorescence
508 intensity along a line drawn across the calyx as described (Sousa et al., 2009; Sedó-Cabezón et al., 2015). Peak
509 fluorescence values were obtained for the inner and outer membrane of all calyces included in one
510 representative section of the epithelium, and average values were obtained per animal. To count synaptic
511 puncta, we imaged the tissues at 0.3 μm intervals to obtain Z-stacks of 2.7 μm. Only HC with their nuclei
512 extending top to bottom of the stack were used for counting, so the counts obtained were from a thick slice
513 from the middle region of the cell, not the whole cell. We counted presynaptic Ribeye/CtBP2 puncta,
514 postsynaptic PSD95 puncta, and pairs of Ribeye and PSD95 puncta that overlapped or were closely apposed (co-
515 localization). For each animal, average counts were obtained from a minimum of 30 HC.

516 Human samples were observed as whole mounts. The tissues were completely examined with the 40X and 63X
517 objectives. Representative Z-stacks, encompassing the entire thickness of the sensory epithelium, were obtained
518 from both striola and peripheral regions. The full stacks were thoroughly studied to determine the presence of
519 pathological features. This included colour channel splitting and merging, observation at several different
520 contrast and brightness adjustments, 3D reconstructions, maximum intensity projection of stacks or sub-stacks
521 and orthogonal projections. Images in Fig. 10 were prepared for illustration purposes only.

522 **Data analysis**

523 Data show mean +/- standard error of the mean except where indicated. Body weight and behavioural data
524 were analysed with repeated-measures MANOVA (Wilks' criterion) with the day as the within-subject factor.
525 Day-by-day analysis was performed after significant day-by treatment interactions were recorded. Other data
526 were analysed by appropriate ANOVA designs and Duncan's post-hoc test, or by Student's t-test. The IBM SPSS
527 Statistics 25 program package was used.

528 **REFERENCES**

529 Anniko, M., Takada, A. and Schacht, J. (1982) Comparative ototoxicities of gentamicin and netilmicin in three
530 model systems. *Am. J. Otolaryngol.* 3, 422-33.

531 Beisel, K.W., Rocha-Sanchez, S.M., Morris, K.A., Nie, L., Feng, F., Kachar, B., Yamoah, E.N. and Fritzsch, B (2005)
532 Differential expression of KCNQ4 in inner hair cells and sensory neurons is the basis of progressive high-
533 frequency hearing loss. *J. Neurosci.* 25, 9285–9293.

534 Benkafadar, N., Janesick, A., Scheibinger, M., Ling, A. H., Jan, T. A. and Heller, S. (2021). Transcriptomic
535 characterization of dying hair cells in the avian cochlea. *Cell Rep.* 34, 108902. doi:
536 10.1016/j.celrep.2021.108902

537 Black, F.O., Gianna-Poulin, C. and Pesznecker, S.C. (2001). Recovery from vestibular ototoxicity. *Otol. Neurotol.*
538 22, 662-671.

539 Black, F.O., Pesznecker, S. and Stallings, V. (2004). Permanent gentamicin vestibulotoxicity. *Otol. Neurotol.* 25,
540 559-569.

541 Breglio, A. M., Rusheen, A. E., Shide, E. D., Fernandez, K. A., Spielbauer, K. K., McLachlin, K. M., Hall, M. D.,
542 Amable, L. and Cunningham, L. L. (2017). Cisplatin is retained in the cochlea indefinitely following
543 chemotherapy. *Nat. Commun.* 8, 1654.

544 Burns, J. C., Kelly, M. C., Hoa, M., Morell, R. J. and Kelley, M. W. (2015). Single-cell RNA-Seq resolves cellular
545 complexity in sensory organs from the neonatal inner ear. *Nat. Commun.* 6, 8557. doi:
546 10.1038/ncomms9557

547 Dechesne, C.J., Winsky, L., Kim, H.N., Goping, G., Vu, T.D., Wenthold, R.J. and Jacobowitz, D.M. (1991)
548 Identification and ultrastructural localization of a calretinin-like calcium-binding protein (protein 10) in the
549 guinea pig and rat inner ear. *Brain. Res.* 560, 139-148.

550 Dilwali, S., Landegger, L. D., Soares, V. Y., Deschler, D. G. and Stankovic, K. M. (2015). Secreted factors from
551 human vestibular schwannomas can cause cochlear damage. *Sci. Rep.* 5, 18599. doi: 10.1038/srep18599

552 Furness, D.N. (2015). Molecular basis of hair cell loss. *Cell Tissue Res.* 361, 387-399.

553 Granados, O. and Meza, G. (2005). Streptidine, a metabolic derivative produced after administration of
554 streptomycin in vivo, is vestibulotoxic in rats. *Histol. Histopathol*. 20, 357-364.

555 Greguske, E.A., Carreres-Pons, M., Cutillas, B., Boadas-Vaello, P. and Llorens, J. (2019) Calyx junction
556 dismantlement and synaptic uncoupling precede hair cell extrusion in the vestibular sensory epithelium
557 during sub-chronic 3,3'-iminodipropionitrile ototoxicity in the mouse. *Arch. Toxicol.* 93, 417-434.

558 Hasson, T., Gillespie, P.G., Garcia, J.A., MacDonald, R.B., Zhao, Y., Yee, A.G., Mooseker, M.S., Corey, D.P. (1997)
559 Unconventional myosins in inner-ear sensory epithelia. *J. Cell. Biol.* 137, 1287-1307.

560 Hirose, K., Westrum, L.E., Stone, J.S., Zirpel, L. and Rubel, E.W. (1999) Dynamic studies of ototoxicity in mature
561 avian auditory epithelium. *Ann. N.Y. Acad. Sci*. 884, 389-409.

562 Hirvonen, T.P., Minor, L.B., Hullar, T.E. and Carey, J.P. (2005). Effects of intratympanic gentamicin on vestibular
563 afferents and hair cells in the chinchilla. *J. Neurophysiol*. 93, 643-655.

564 Hunt, M.A., Miller, S.W., Nielson, H.C. and Horn, K.M. (1987) Intratympanic injections of sodium arsanilate
565 (atoxil) solution results in postural changes consistent with changes described for labyrinthectomized rats.
566 *Behav. Neurosci.* 101, 427–428.

567 Imamura, S., and Adams, J.C. (2003) Distribution of gentamicin in the guinea pig inner ear after local or systemic
568 application. *J. Assoc. Res. Otolaryngol.* 4, 176-195.

569 Jiang, H., Sha, S. H., Forge, A. and Schacht, J. (2006). Caspase-independent pathways of hair cell death induced
570 by kanamycin in vivo. *Cell Death Differ.* 13, 20–30.

571 Katsumi, S., Sahin, M. I., Lewis, R. M., Iyer, J. S., Landegger, L. D., & Stankovic, K. M. (2020). Intracochlear
572 perfusion of tumor necrosis factor-alpha induces sensorineural hearing loss and synaptic degeneration in
573 guinea pigs. *Front. Neurol.* 10, 1353.

574 Kohonen, A. and Tarkkanen, J. (1969) Cochlear damage from ototoxic antibiotics by intratympanic application.
575 *Acta Otolaryngol.* 68, 90-97.

576 Li, L., Nevill, G. and Forge, A. (1995). Two modes of hair cell loss from the vestibular sensory epithelia of the
577 guinea pig inner ear. *J. Comp. Neurol*. 355, 405-417.

578 Llorens, J. and Rodríguez-Farré, E. (1997). Comparison of behavioral, vestibular, and axonal effects of subchronic
579 IDPN in the rat. *Neurotoxicol. Teratol*. 19, 117-127.

580 Llorens, J., Demêmes, D. and Sans, A. (1993). The behavioral syndrome caused by 3,3'-iminodipropionitrile and
581 related nitriles in the rat is associated with degeneration of the vestibular sensory hair cells. *Toxicol. Appl.*
582 *Pharmacol.* 123, 199-210.

583 Lopez, I., Honrubia, V., Lee, S.C., Schoeman, G. and Beykirch, K. (1997) Quantification of the process of hair cell
584 loss and recovery in the chinchilla crista ampullaris after gentamicin treatment. *Int. J. Dev. Neurosci.* 15,
585 447-461.

586 Lopez-Escamez, J.A., Carey, J., Chung, W.H., Goebel, J.A., Magnusson, M., Mandala, M., Newman-Toker, D.E.,
587 Strupp, M., Suzuki, M., Trabalzini, F. and Bisdorff, A. (2015) Diagnostic criteria for Menière's disease. *J.*
588 *Vestib. Res.* 25, 1-7.

589 Lysakowski, A., Gaboyard-Niay, S., Calin-Jageman, I., Chatlani, S., Price, S.D. and Eatock, R.A. (2011). Molecular
590 microdomains in a sensory terminal, the vestibular calyx ending. *J. Neurosci*. 31, 10101–10114.

591 Maroto, A. F., Barrallo-Gimeno, A. and Llorens, J. (2021a). Relationship between vestibular hair cell loss and
592 deficits in two anti-gravity reflexes in the rat. Hear. Res. 410, 108336. doi: 10.1016/j.heares.2021.108336

593 Maroto, A.F., Greguske, E.A., Barrallo-Gimeno, A. and Llorens, J. (2021b) Evaluation of cellular and molecular
594 pathology in the rodent vestibular sensory epithelia by immunofluorescent staining and confocal
595 microscopy. In: E*xperimental Neurotoxicology Methods, Neuromethods, vol. 172*, Llorens, J. and Barenys.
596 M., Editors. Springer US, pp 35-50.

597 Maroto, A.F., Greguske, E.A., Deulofeu, M., Boadas-Vaello, P. and Llorens, J. (2021c) Behavioral assessment of
598 vestibular dysfunction in rats. In: E*xperimental Neurotoxicology Methods, Neuromethods, vol. 172*, Llorens,
599 J. and Barenys. M., Editors. Springer US, pp 199-215.

600 Martins-Lopes, V., Bellmunt, A., Greguske, E.A., Maroto, A.F., Boadas-Vaello, P. and Llorens, J. (2019)
601 Quantitative assessment of anti-gravity reflexes to evaluate vestibular dysfunction in rats. *J. Assoc. Res.*
602 *Otolaryngol.* 20, 553-563.

603 McInturff, S., Burns, J.C., Kelley, M.W. (2018) Characterization of spatial and temporal development of Type I
604 and Type II hair cells in the mouse utricle using new cell-type-specific markers. *Biol. Open* 7, bio038083.
605 doi: 10.1242/bio.038083.

606 Murillo-Cuesta, S., Contreras, J., Cediel, R. and Varela-Nieto, I. (2010) Comparison of different aminoglycoside
607 antibiotic treatments to refine ototoxicity studies in adult mice. *Lab. Anim.* 44, 124-131.

608 Nakagawa, T., Yamane, H., Shibata, S. and Nakai, Y. (1997) Gentamicin ototoxicity induced apoptosis of the
609 vestibular hair cells of guinea pigs. *Eur. Arch. Otorhinolaryngol.* 254, 9-14.

610 Nakayama, M., Riggs, L.C. and Matz, G.J. (1996) Quantitative study of vestibulotoxicity induced by gentamicin or
611 cisplatin in the guinea pig. *Laryngoscope* 106, 162-167.

612 Oesterle, E.C., Campbell, S., Taylor, R.R., Forge, A. and Hume, C.R. (2008) Sox2 and JAGGED1 expression in
613 normal and drug-damaged adult mouse inner ear. *J. Assoc. Res. Otolaryngol.* 9, 65-89.

614 Pellis, S.M., Pellis, V.C. and Teitelbaum, P. (1991) Labyrinthine and other supraspinal inhibitory controls over
615 head-and-body ventroflexion. *Behav. Brain Res*. 46, 99-102.

616 Rubel, E.W., Furrer, S.A. and Stone, J.S. (2013). A brief history of hair cell regeneration research and speculations
617 on the future. *Hear Res*. 297, 42-51.

618 Schirmer, M., Kaiser, A., Lessenich, A., Lindemann, S., Fedrowitz, M., Gernert, M. and Löscher, W. (2007).
619 Auditory and vestibular defects and behavioral alterations after neonatal administration of streptomycin to
620 Lewis rats: Similarities and differences to the circling (ci2/ci2) Lewis rat mutant. *Brain Res*. 1155, 179–195.

621 Sedó-Cabezón, L., Jedynak, P., Boadas-Vaello, P. and Llorens, J. (2015) Transient alteration of the vestibular
622 calyceal junction and synapse in response to chronic ototoxic insult in rats. *Dis. Model. Mech.* 8, 1323-1337.

623 Seoane, A., Demêmes, D. and Llorens, J. (2001a). Relationship between insult intensity and mode of hair cell loss
624 in the vestibular system of rats exposed to 3,3'-iminodipropionitrile. *J. Comp. Neurol.* 439, 385-399.

625 Seoane, A., Demêmes, D. and Llorens, J. (2001b). Pathology of the rat vestibular sensory epithelia during
626 subchronic 3,3'-iminodipropionitrile exposure: hair cells may not be the primary target of toxicity. *Acta*
627 *Neuropathol*. 102, 339-348.

628 Sousa, A.D., Andrade, L.R., Salles, F.T., Pillai, A.M., Buttermore, E.D., Bhat, M.A. and Kachar, B (2009). The
629 septate junction protein caspr is required for structural support and retention of KCNQ4 at calyceal synapses
630 of vestibular hair cells. *J. Neurosci*. 29, 3103-3108.

631 Sullivan, M. J., Rarey, K. E. and Conolly, R. B. (1987). Comparative ototoxicity of gentamicin in the guinea pig and
632 two strains of rats. Hear. Res. 31, 161–167.

633 Sultemeier, D. R. and Hoffman, L. F. (2017). Partial aminoglycoside lesions in vestibular epithelia reveal broad
634 sensory dysfunction associated with modest hair cell loss and afferent calyx retraction. Front. Cell. Neuorsci.
635 11, 331.

636 Taylor, R.R., Nevill, G. and Forge, A. (2008) Rapid hair cell loss: a mouse model for cochlear lesions. *J. Assoc. Res.*
637 *Otolaryngol.* 9, 44-64.

638 von Brevern, M., Bertholon, P., Brandt, T., Fife, T., Imai, T., Nuti, D. and Newman-Toker, D. (2015) Benign
639 paroxysmal positional vertigo: Diagnostic criteria. *J. Vestib. Res.* 25, 105-117-

640 Wu, W.J., Sha, S.H., McLaren, J.D., Kawamoto, K., Raphael, Y. and Schacht, J. (2001) Aminoglycoside ototoxicity
641 in adult CBA, C57BL and BALB mice and the Sprague-Dawley rat. *Hear. Res.* 158; 165-178.

642 LEGENDS FOR FIGURES

643 **Figure 1.** Effects of sub-chronic streptomycin on the tail-lift reflex of rats. Data are mean ± SE minimum angles
644 formed by the nose, the back of the neck, and the base of the tail during the reflex behaviour elicited by a tail-
645 lift manoeuvre. Loss of vestibular function causes loss of the anti-gravity trunk extension reflex, which results in
646 ventral curling and thus in smaller angles. **A.** Effects of one injection per day at 0 (CTRL, vehicle control) or 500
647 mg/kg (STR-500) of streptomycin for 6 weeks, starting at 21 days of age. * $p<0.05$, different from control group
648 after significant day by treatment interaction effect in repeated-measures MANOVA. **B.** Effects of two injections
649 per day at 0 (CTRL, vehicle control), 300 (STR-300x2), 350 (STR-350x2), or 400 (STR-400x2) mg/kg of
650 streptomycin for 6, 6, 4, or 3 weeks, respectively, starting at 21 days of age. The numbers of animals were
651 reduced to 6 in the CTRL group after day 28, and to 7 in the STR-300x2 and STR-350x2 groups after day 21. **a, b,**
652 **c, d**: groups with different letters are significantly different ($p<0.05$), Duncan's test after significant ANOVA on
653 that day. **C.** Recovery of the tail-lift reflex after the end of exposure in rats administered once a day with 500
654 mg/kg (STR-500) of streptomycin for 6 weeks. **D.** Loss and recovery of the tail-lift reflex in two individual rats
655 administered twice a day with 350 (STR-350) or 400 mg/kg (STR-400) of streptomycin for 3 weeks, followed by 3
656 weeks of washout..

657 **Figure 2.** Effects of sub-chronic streptomycin on the vestibular sensory epithelium of the rat as observed in
658 surface preparations of saccules examined by SEM. **A.** Control saccule, showing a high and uniform density of
659 stereocilia bundles throughout the macula. **B.** Effect of one injection per day of 500 mg/kg of streptomycin (STR-
660 500) for 8 weeks. A reduced density of stereocilia bundles is noticeable at this low magnification. The boxed area
661 is shown at higher magnification in panel C. **C.** Higher magnification of the saccule shown in panel B. Note the
662 areas where the lack of stereocilia bundles is evident (arrows). **D and E.** High magnification views of a saccule
663 from a STR-500 rat at 6 weeks of treatment. Note the contacts between the apical edges of supporting cells,
664 marked by a high density of microvellosities, denoting the lack of stereocilia bundles (star), and the bundles

665 showing stereocilia fusion and HC protrusion into the luminal cavity (arrows). **Scale Bars:** 100 μm in **A** and **B**; 20
666 μm in **C**; 2 μm in **D**; 5 μm in **E**.

667 **Figure 3.** Effect of sub-chronic streptomycin on the numbers of HCI and HCII in the vestibular epithelia of the rat.
668 **A, B, C**. Effect of 500 mg/kg of streptomycin, once a day, for 6 or 8 weeks, as recorded at the end of the
669 exposure period or at the end of a washout period of 8 weeks after treatment. Vestibular cristae, utricles and
670 saccules were immunolabelled with anti-MYO7A (red, to label all HCs), anti-CASPR1 (green, to identify HCI) and
671 anti-calretinin (blue, to label HCII) antibodies, and examined by confocal microscopy. The central/striola and
672 peripheral regions of the epithelia were evaluated separately. **A**. Representative images from the peripheral
673 utricle of a vehicle control rat, a rat treated with streptomycin for 8 weeks (STR-500 8wk), and a washout (STR-
674 500 WO) rat. HCI were defined by MYO7A+ cells with adjacent CASPR1 label, even if thin or fragmented, and no
675 calterinin label (arrows). Note the fragmentation of the CASPR1 label in the STR-500 (8wk) rat. **Scale bar**: 20 μm.
676 **B and C.** Counts of HCI **(B)** and HCII **(C)** cells. Data are mean number of cells +/- SE per section. For each animal
677 and epithelial zone, numbers were obtained by averaging counts from 8 confocal stacks from a representative
678 histological section. **D, E**. Effect of 300 (STR-300x2), 350 (STR-350x2) or 400 (STR-400x2) mg/kg of streptomycin,
679 twice a day, for 6, 4, or 3 weeks. The washout (WO) group includes animals allowed 3 weeks of recovery after
680 receiving STR-350x2 or STR-400x2 for 3 or 4 weeks. Vestibular cristae were labelled with anti-SPP1 (blue, to label
681 HCI), anti-CASPR1 (green) and anti-calretinin (red) antibodies. HCI were defined as SPP1+ cells and HCII were
682 cells with calretinin label. **D.** Partial view of representative sections of control and streptomycin cristae. **Scale**
683 **bar**: 20 μm. **E.** Relative numbers of HCI and HCII in the crista sections. Data are mean number of cells +/- SE per
684 transversal section, including central and peripheral regions. In **B**, **C**, and **E**, the number of replicas in the figure
685 legends indicate minimum/maximum number of animals counted per epithelium and zone in the treatment
686 group. **a, b, c, ab**: groups not sharing a letter are different ($p<0.05$), Duncan's multiple-comparisons test after
687 significant ($p<0.05$) one-way ANOVA. **(n.s.):** non-significant ($p>0.05$) group differences in the ANOVA analysis.

688 **Figure 4.** Effects of sub-chronic streptomycin on the expression of CASPR1 in the central/striola (C/S) and
689 peripheral (P) regions of the vestibular crista, utricle and saccule of the rat. The samples were labelled with anti-
690 MYO7A (red), anti-CASPR1 (green) and anti-calretinin (blue) antibodies. **A.** Representative images from mid-
691 crista sections from a CTRL rat (**a** to **d**), a rat treated with 500 mg/kg of streptomycin, once a day, for 6 weeks (**e**
692 to **h**), and a rat allowed recovery during a washout period of 10 weeks after the streptomycin treatment (**i** to **l**).
693 Note the loss and fragmentation of the CASPR1 label caused by streptomycin and its recovery after washout.
694 The intensity of MYO7A label also decreased and recovered. **B.** Quantitative analysis of the CASPR1
695 fluorescence. Data are normalised arbitrary fluorescence amount per cell +/- SE. For each animal, epithelium
696 and zone, the average amount of fluorescence was obtained from all HCs available for analysis up to 40 cells.
697 Numbers below the bars indicate number of animals included per group. **a, b**: groups not sharing a letter are
698 different ($p<0.05$), Duncan's multiple-comparisons test after significant ($p<0.05$) one-way ANOVA.

699 **Figure 5.** Effects of sub-chronic streptomycin on the expression of synaptic proteins in the HCI and calyx
700 afferents of the rat. **A.** Redistribution of KCNQ4 in the inner and outer membranes of the calyx terminals
701 afferent to HCI. Vestibular crista were labelled with anti-CASPR1 (green) and anti-KCNQ4 (red) antibodies. The
702 asterisk indicates a calyx with a control-like co-localisation of CASPR1 and KCNQ4 in the inner membrane of the
703 calyx. The arrowhead points to a calyx with CASPR1 loss and reduced co-localisation, with the KCNQ4 antibody
704 labelling a greater area than the CASPR1 antibody. The arrow points to the outer membrane of a calyx with
705 greatly reduced CASPR1 label and redistribution of KCNQ4 throughout both the inner (i and i') and outer (o and
706 o') membranes. **B.** Quantitative analysis of the distribution of KCNQ4 label in the inner and outer face of the
707 calyces in crista from control rats (CTRL), rats treated with 500 mg/kg of streptomycin (STR-500), once a day, for
708 6 or 8 weeks, and rats allowed recovery during a washout period of 8-10 weeks after the streptomycin
709 treatment. Note that control and washout animals do not display KCNQ4 in the outer face membrane. Data are
710 mean arbitrary fluorescence units +/- SE. The number of replicas indicate the number of animals included in the
711 analysis per group. **a, b**: groups not sharing a letter are different ($p<0.05$), Duncan's multiple-comparisons test

712 after significant ($p<0.05$) one-way ANOVA. **C.** Labelling of pre-synaptic (Ribeye, red) and post-synaptic (PSD-95,
713 green) proteins on HCs (MYO7A, white) in vestibular crista. In subpanel **c1**, the MYO7A label is included to show
714 HC bodies in a control crista. Subpanel **c2** shows the same image without the MYO7A label but including lines
715 delineating the limits of two HCs and arrows pointing to examples of pairs of ribeye and PSD-95 puncta. **D.**
716 Effects of sub-chronic streptomycin on the numbers of synaptic puncta per 2.7 μm-tick optical sections of HCs.
717 Data are mean number of pre-synaptic and post-synaptic puncta, as well as pre- and post-synaptic pairs (Co-
718 localization), +/- SE, from control rats (CTRL) and rats treated with 500 mg/kg of streptomycin (STR-500), once a
719 day, for 6 weeks. The number of replicas indicate the number of animals included in the analysis per group. *: $p<$
720 0.05, and ***: $p<0.001$, CTRL versus STR-500, Student's T-test.

721 **Figure 6.** Effects of sub-chronic streptomycin on the calyceal junction and calyx integrity as observed by TEM. **A.**
722 Control crista. The calyceal junction is revealed by the high electron density of the apposing membranes (long
723 arrows) of HCI and inner side of the calyx (c), higher than that found in the outer side of the calyx (arrowheads).
724 **B.** Crista of a rat exposed to 500 mg/kg of streptomycin, once a day, for 6 weeks. In most of the area where the
725 calyceal junction should be found, the apposing membranes show a low electron density (short arrows), similar
726 to that in the outer face of the calyx (arrowhead). **C.** Higher magnification of the calyceal junction (long arrow)
727 and the outer side of the calyx (arrowhead) in a control saccule. **D.** Higher magnification from a crista of a rat
728 exposed to 500 mg/kg of streptomycin, once a day, for 6 weeks. Note the short segment of calyceal junction
729 (long arrow) that remains together with areas devoid of it (short arrow) and the similarity between the latter
730 and the membranes in the outer side of the calyx (arrowheads). **E.** Calyceal junction dismantlement and calyx
731 fragmentation in a HCI showing evidence of ongoing extrusion, from a utricle of a rat exposed to 300 mg/kg of
732 streptomycin, twice a day, for 6 weeks. Note the absence of calyceal junction (short arrows), the fragmentation
733 of the calyx (c, green shadow), and the direct contact between supporting cells and the HCI (stars). The purple
734 shadow highlights one supporting cell (sc). **F.** Higher magnification of the boxed area in panel **E**. Note the
735 similarity of the membranes between the place where the calyceal junction is missing (short arrows) and the

736 outer side of the calyx (arrowheads). Note also the direct contact between a supporting cell (sc) and the HCI
737 (star). **Scale Bars: A**, **B**, and **E**, 2 mm; **C**, **D**, and **F**, 1 mm.

738 **Figure 7.** Evidence of HC extrusion in utricles of rats exposed to sub-chronic streptomycin as observed by
739 immunofluorescence and TEM. The images are from rats administered twice a day with 350 mg/kg of
740 streptomycin for 4 weeks, or with 300 mg/kg for 6 weeks. **A.** Utricles immunolabelled with antibodies against
741 MYO7A (red), CASPR1 (green) and radixin (blue). The radixin label of stereocilia and microvilli outlines the
742 surface of the epithelium. Arrowheads point to HCs protruding (**a**, **b**), extruding (**c**, **d**, **e**) or completely extruded
743 (**f**) into the luminal cavity of the utricle. **B** and **C.** TEM images of HCs in a protrusion stage corresponding to that
744 shown in panels **a** and **b**, respectively, of part **A**. Stereocilia (arrows) and striated organelles (arrowheads)
745 identify the extruding cells as HCs. In **B**, note the position of the nucleus of the HC inside the epithelium, and the
746 remnant of a calyx terminal (green shadow) that identifies the HC as a HCI. In **C**, note the position of the nucleus
747 of the HC (unidentified type), half way into the luminal cavity of the utricle. **Scale Bars: A**, 20 mm; **B**, and **C**, 2
748 mm.

749 **Figure 8.** Evaluation of the calyceal junction in vestibular epithelia from patients of vestibular diseases, as
750 revealed by CASPR1 immunolabel (green, light blue when co-localizing with calretinin blue label). In the main
751 panels, HC bodies are labelled with an anti-MYO7A antibody (red). Calretinin is shown in blue in main panels **C** to
752 **F**, and in purple in the inset in **C**. **A**. Epithelium from a patient of Ménière's Disease showing no pathological
753 features. Note the elevated density of HCs and the continuous distribution of the CASPR1 label throughout the
754 calyceal junction area of each HCI. **B.** Epithelium from a meningioma patient, showing also no overt pathology.
755 **C.** Epithelium from a meningioma patient. Note the low density of HCs and the normally continuous CASPR1
756 label in calyces of both calretinin+ calyx-only terminals (arrowhead) and calretinin- dimorphic terminals (short
757 arrow). The **inset** displays the same two calyces; a thinner stack is shown to highlight the uninterrupted CASPR1
758 label and its placement in the inner membrane of the calretinin+ calyx of the calyx-only terminal. **D.** Utricle
759 periphery from a vestibular schwannoma patient. Around different HCI, the calyceal CASPR1 label is found in

760 both normal continuous distribution (arrowhead) and in faint and broken distribution (long arrows). **E.** Striola
761 region of the same utricle in **D**. Although some calyceal junctions display a roughly normal continuous
762 distribution of the CASPR1 label (arrowheads), most display faint, broken or largely absent label (arrows). **F**.
763 Higher magnification image from the same patient in **D** and **E.** Two calyces formed by calyx-only terminals are
764 highlighted, one with continuous CASPR1 label (arrowhead) and the other with a patched distribution of this
765 label (long arrow). **G.** Epithelium from a different vestibular schwannoma patient displaying normal CASPR1
766 distribution in calyces from dimorphic terminals (arrowhead) and a double calyx of a calretinin+ calyx-only
767 terminal displaying a partial CASPR1 label in one HC (short arrow) and no CASPR1 in the other HC (long arrow).
768 **Image thickness: A**, 12 μm; **B**, 10 μm; **C**, main 9.5 μm, inset 5 μm; **D**, 1.6 μm; **E**, 2.6 μm; **F**, 5 μm; **G**, 6 μm. **Scale**
769 **Bars: A**, **C**, **D**, and **E**, 25 μm; **B**, 50 μm; **F**, and **G**, 5 μm.

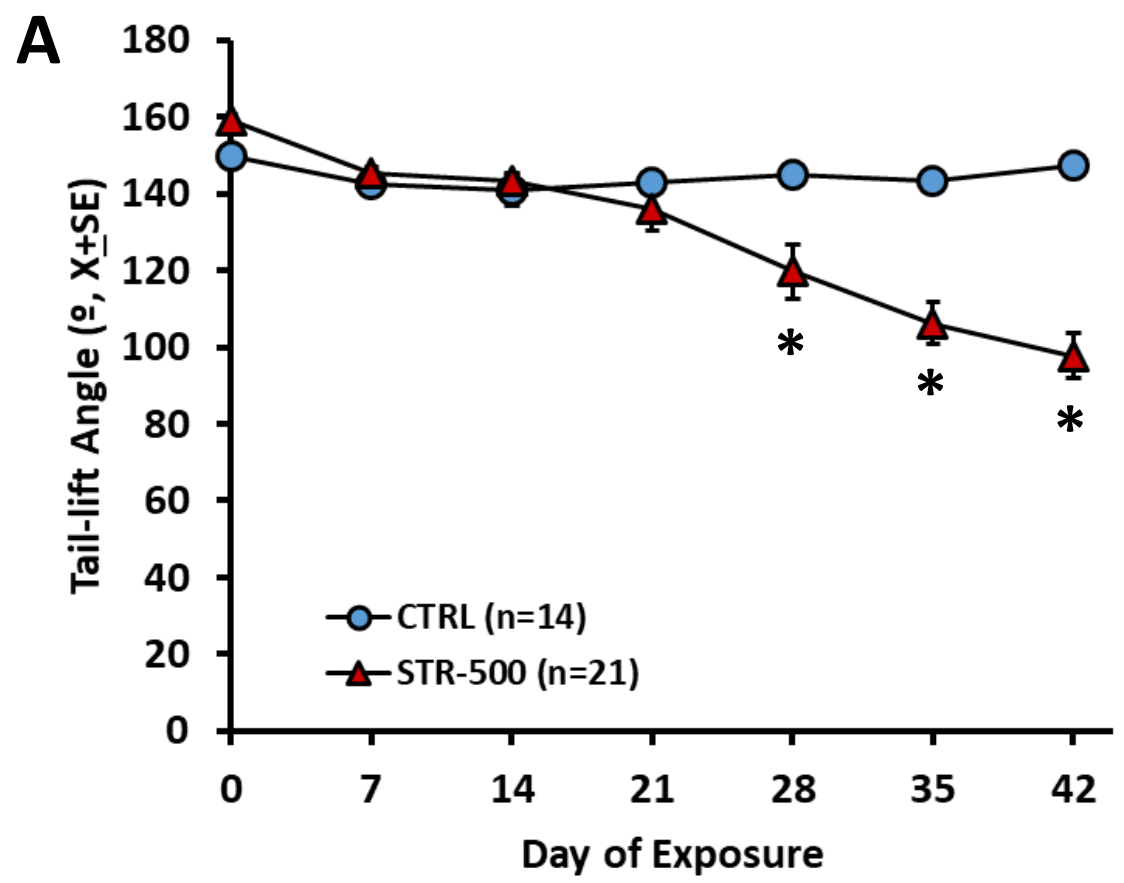
A
Tail-lift Angle (º, X+SE)
Day of Exposure
CTRL (n=14)
STR-500 (n=21)
*
*
*

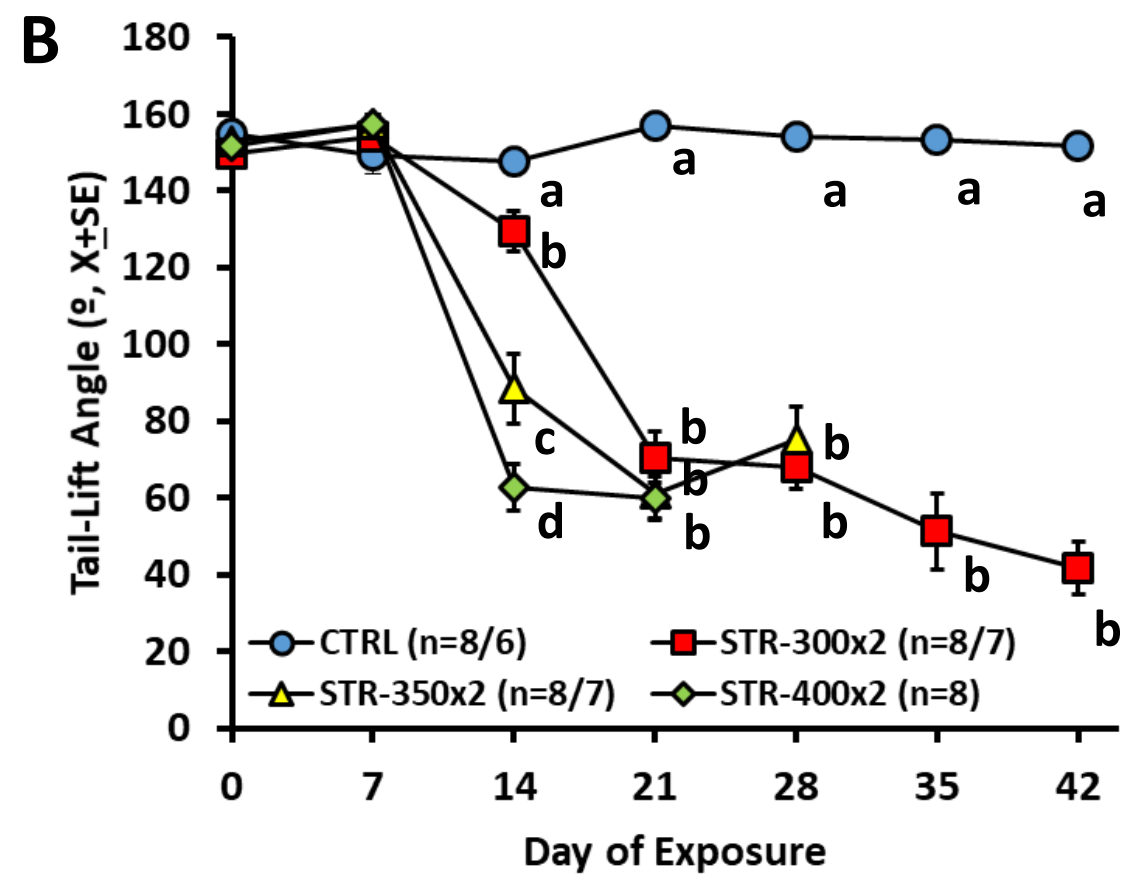
B
Tail-Lift Angle (º, X+SE)
Day of Exposure
CTRL (n=8/6)
STR-300x2 (n=8/7)
STR-350x2 (n=8/7)
STR-400x2 (n=8)
a
b
c
d

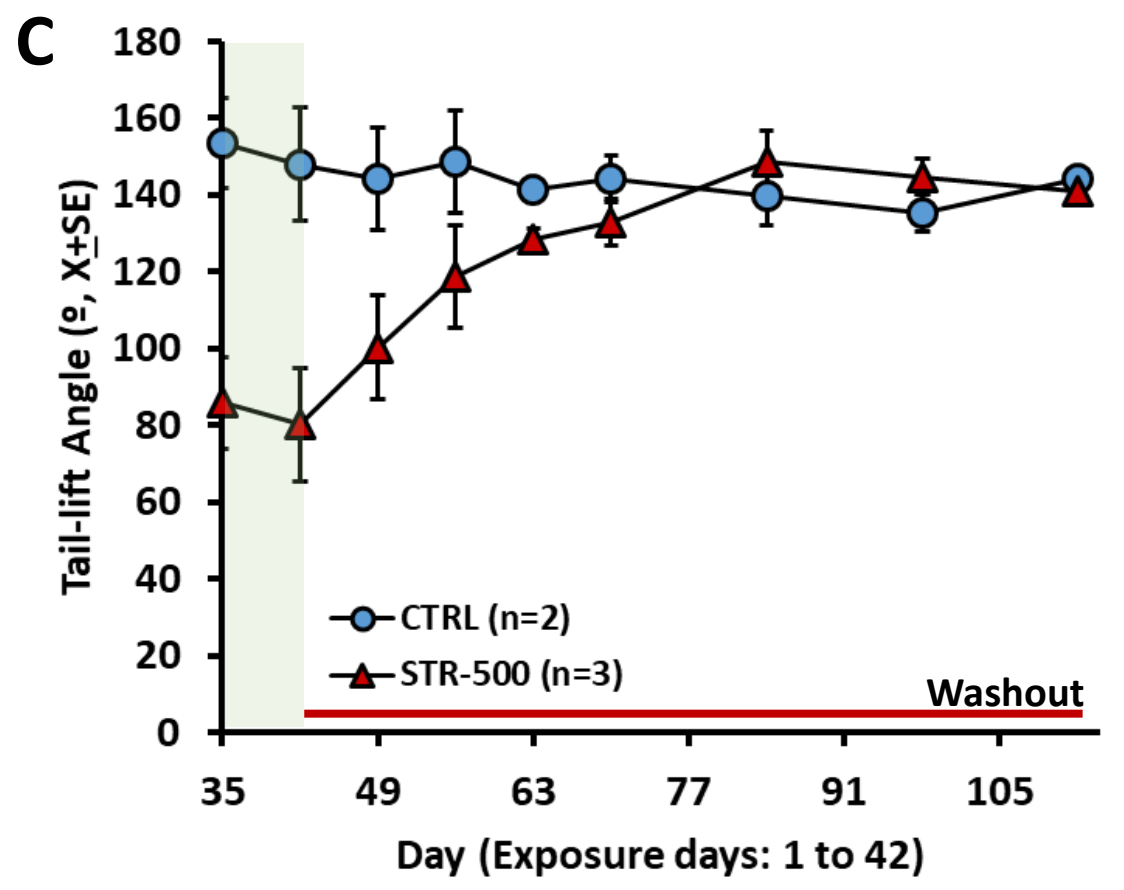
C
Tail-lift Angle (º, X+SE)
Day (Exposure days: 1 to 42)
CTRL (n=2)
STR-500 (n=3)
Washout

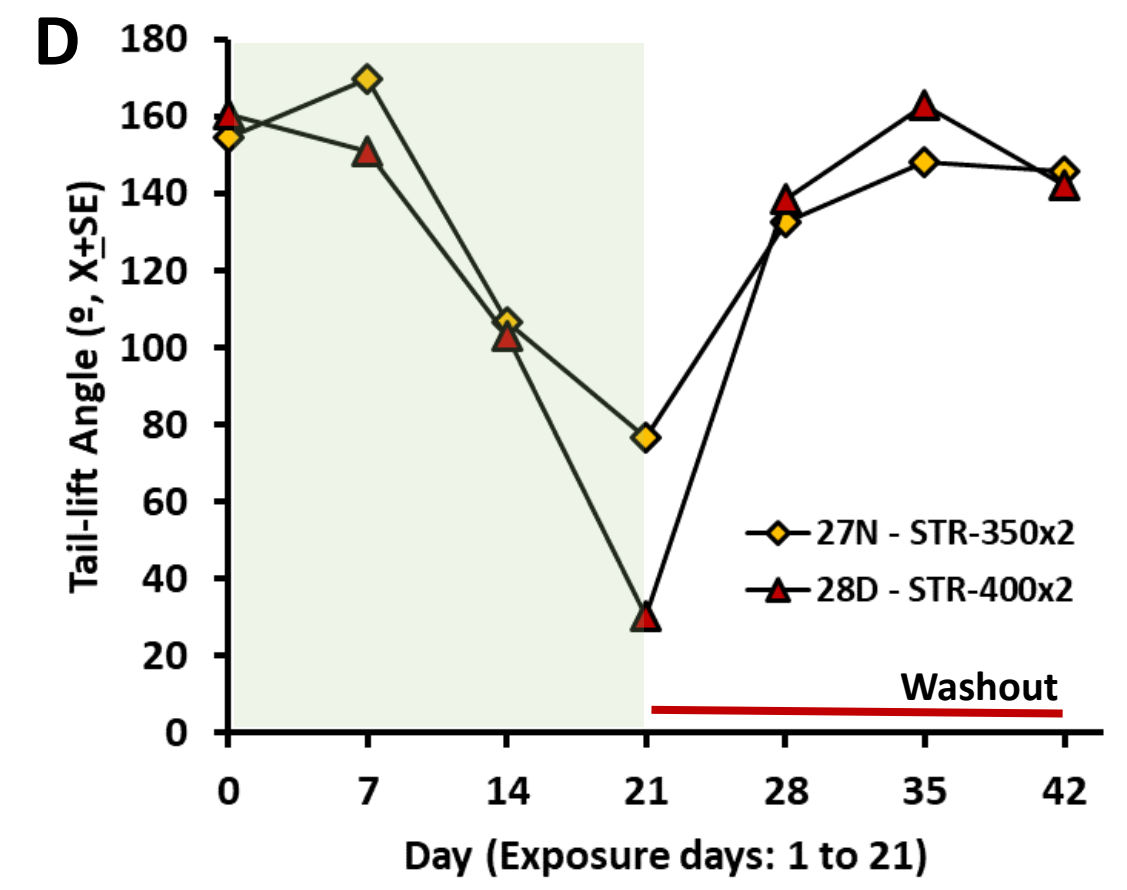
D
Tail-lift Angle (º, X+SE)
Day (Exposure days: 1 to 21)
27N - STR-350x2
28D - STR-400x2
Washout

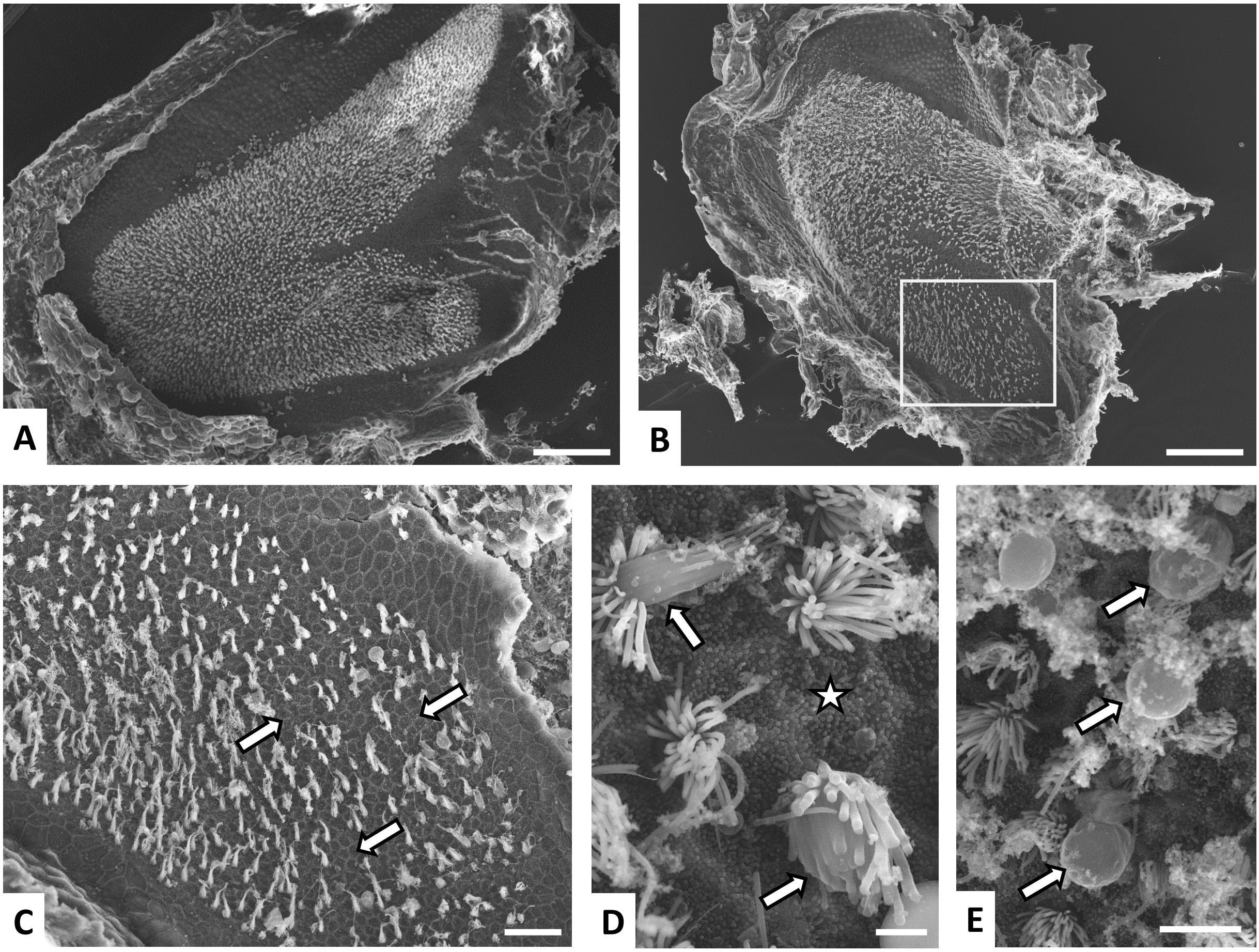
A
B
C
D
E

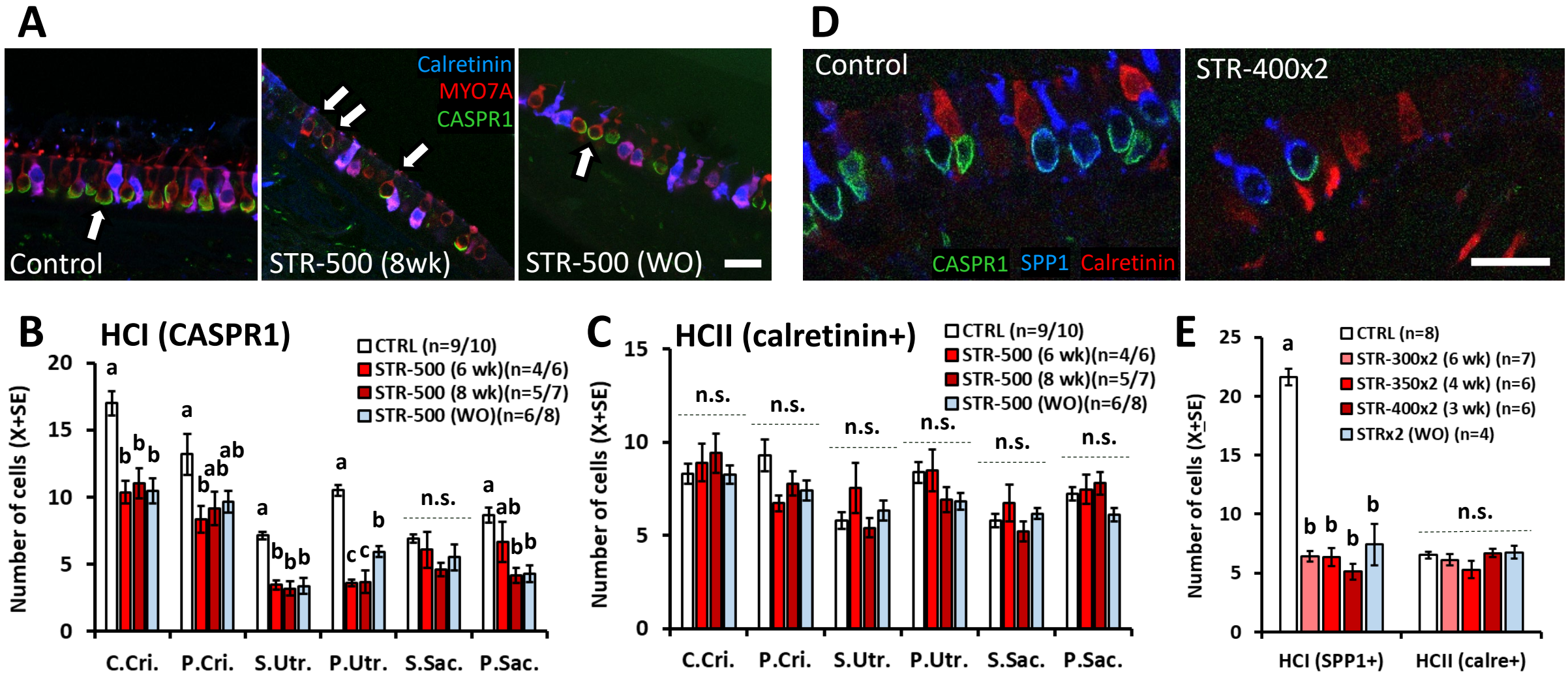
A
Calretinin
MYO7A
CASPR1
Control
STR-500 (8wk)
STR-500 (WO)
D
Control
STR-400x2
CASPR1 SPP1 Calretinin
B
HCI (CASPR1)
CTRL (n=9/10)
STR-500 (6 wk)(n=4/6)
STR-500 (8 wk)(n=5/7)
STR-500 (WO)(n=6/8)
Number of cells (X+SE)
C.Cri. P.Cri. S.Utr. P.Utr. S.Sac. P.Sac.
C
HCII (calretinin+)
n.s.
E
CTRL (n=8)
STR-300x2 (6 wk) (n=7)
STR-350x2 (4 wk) (n=6)
STR-400x2 (3 wk) (n=6)
STRx2 (WO) (n=4)
HCI (SPP1+)
HCII (calre+)

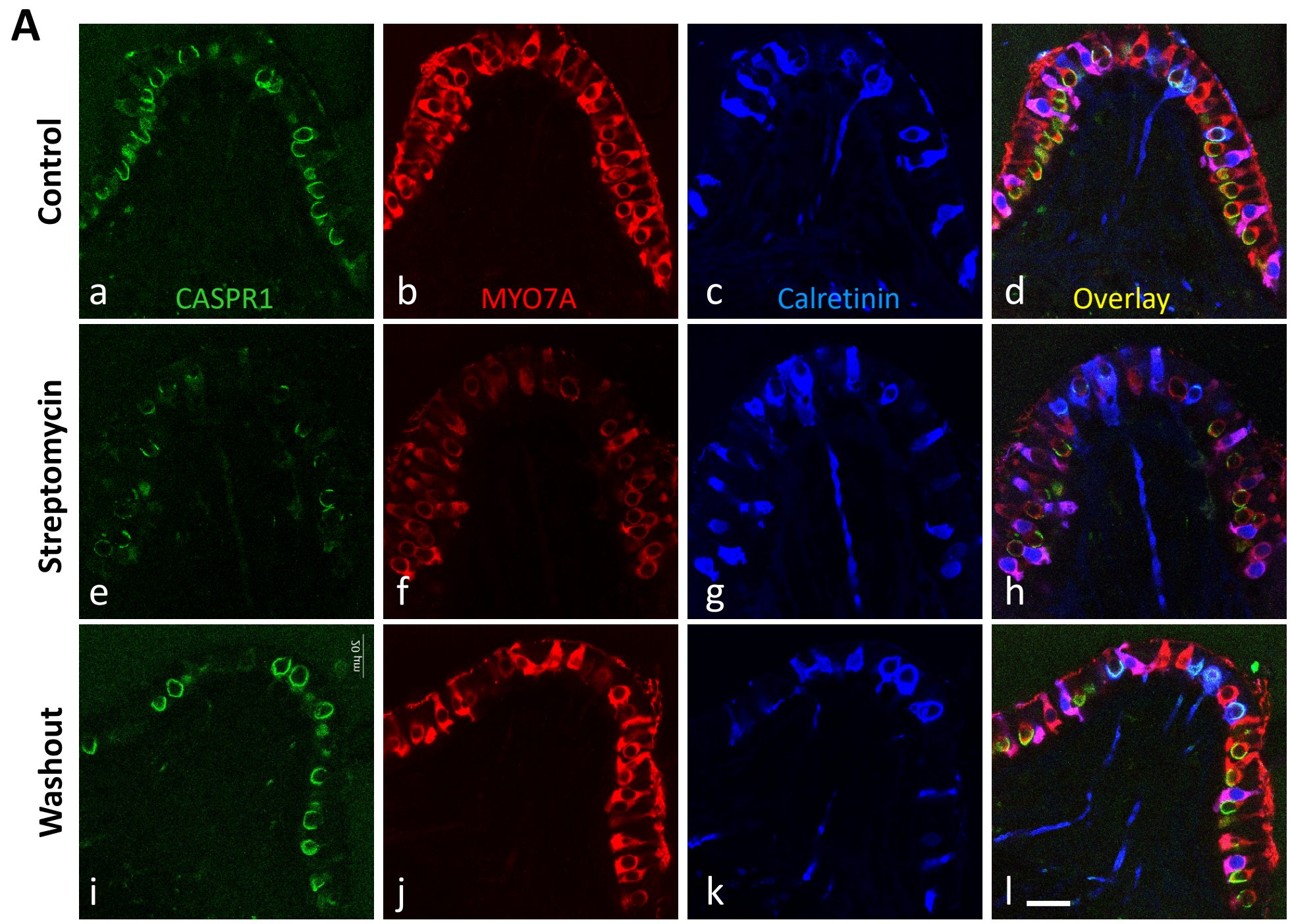
A
Control
Streptomycin
Washout
a
CASPR1
b
MYO7A
c
Calretinin
d
Overlay
e
f
g
h
i
j
k
l
20 µm

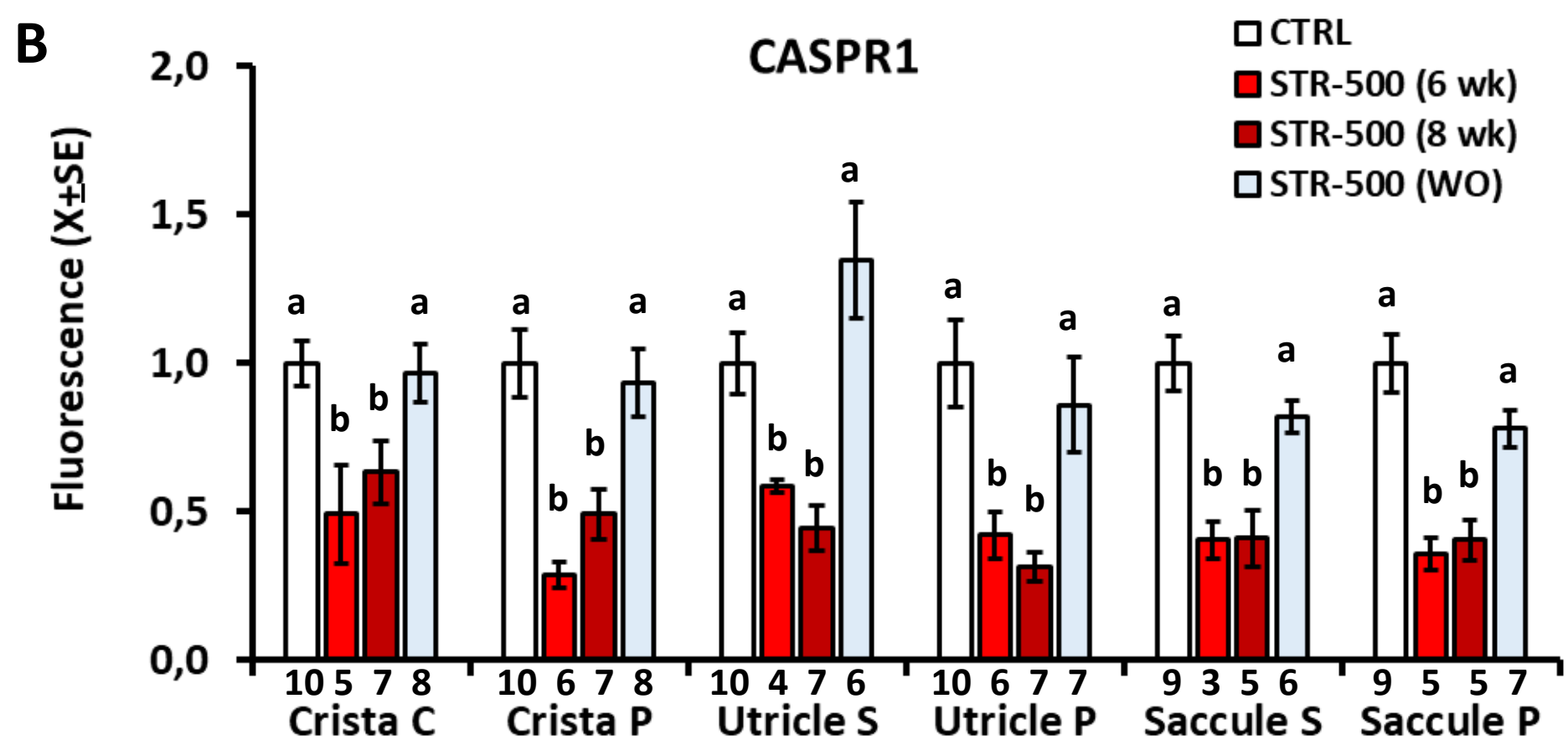
B
CASPR1
CTRL
STR-500 (6 wk)
STR-500 (8 wk)
STR-500 (WO)
Fluorescence (X±SE)
2,0
1,5
1,0
0,5
0,0
10 5 7 8
10 6 7 8
10 4 7 6
10 6 7 7
9 3 5 6
9 5 5 7
Crista C
Crista P
Utricle S
Utricle P
Saccule S
Saccule P

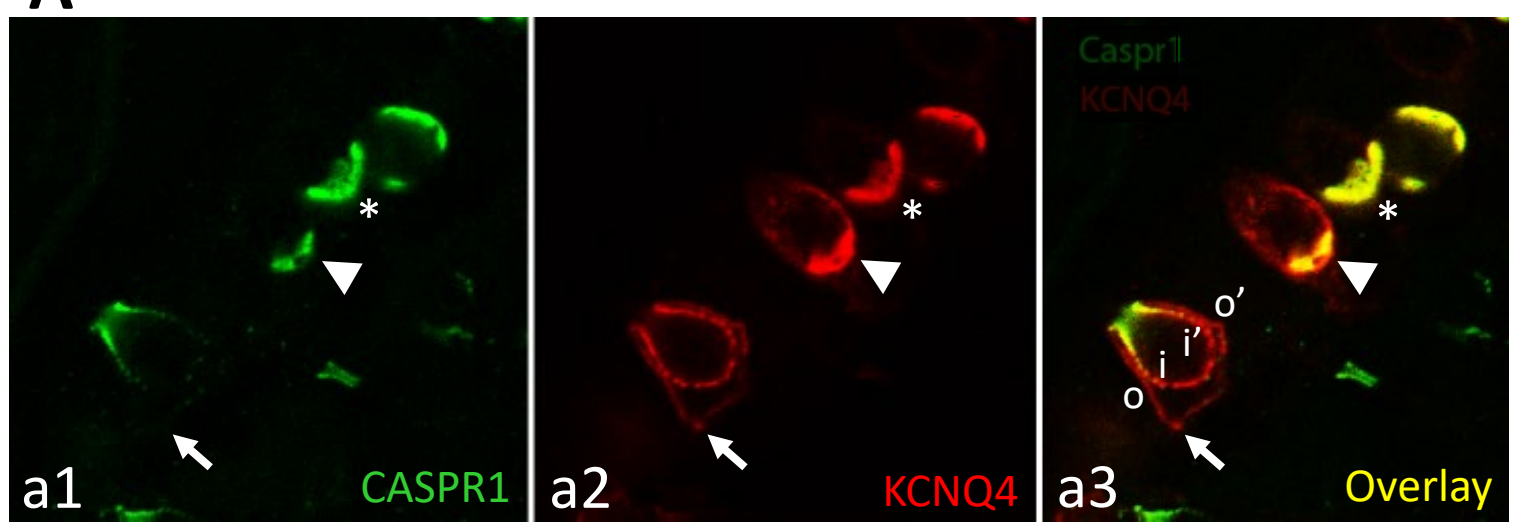
A
Caspr1
KCNQ4
*
o'
i'
i
o
a1
CASPR1
a2
KCNQ4
a3
Overlay

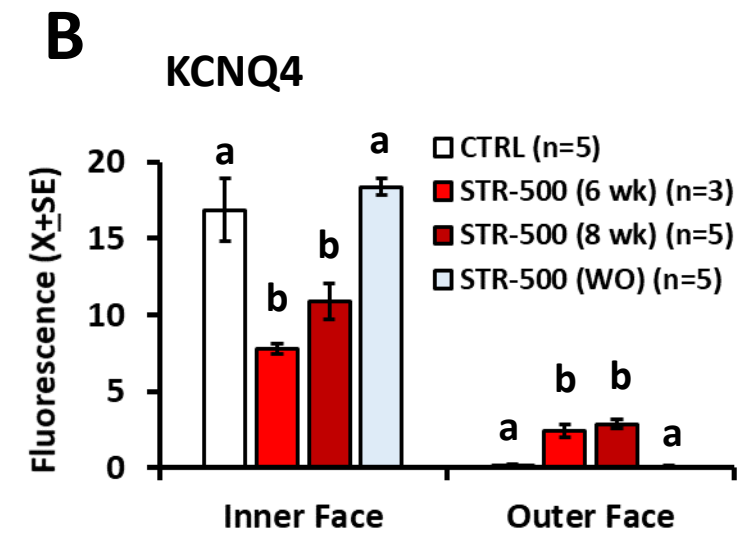
B
KCNQ4
Fluorescence (X±SE)
20
15
10
5
0
a
b
b
a
a
b
b
a
CTRL (n=5)
STR-500 (6 wk) (n=3)
STR-500 (8 wk) (n=5)
STR-500 (WO) (n=5)
Inner Face
Outer Face

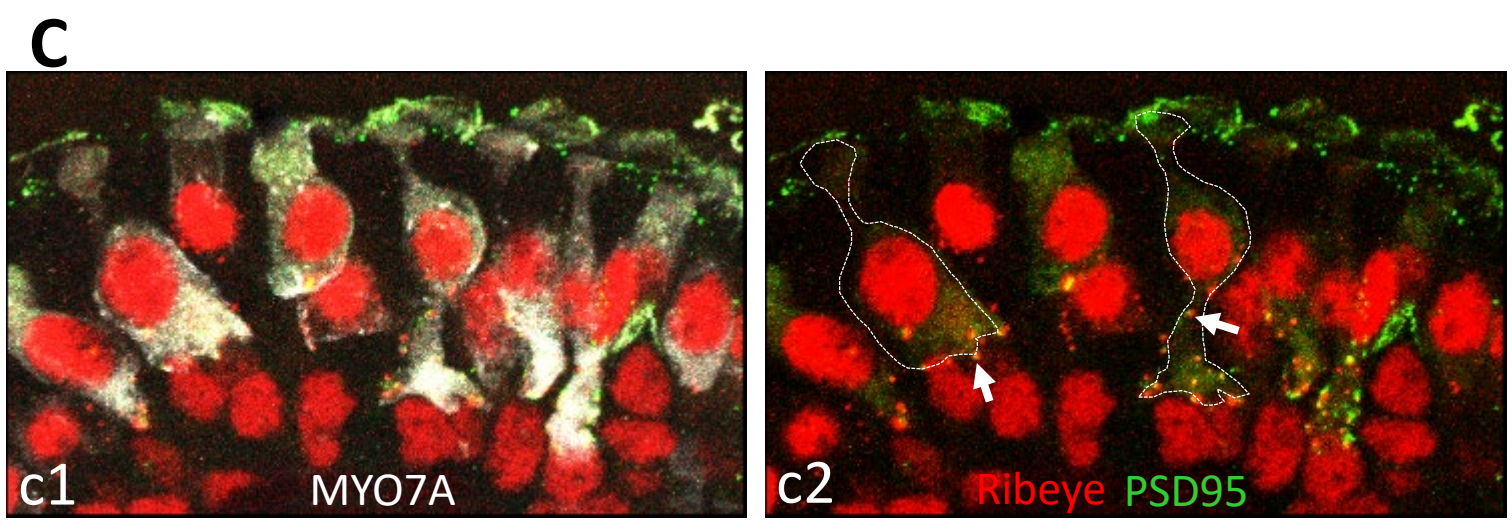
C
c1
MYO7A
c2
Ribeye
PSD95

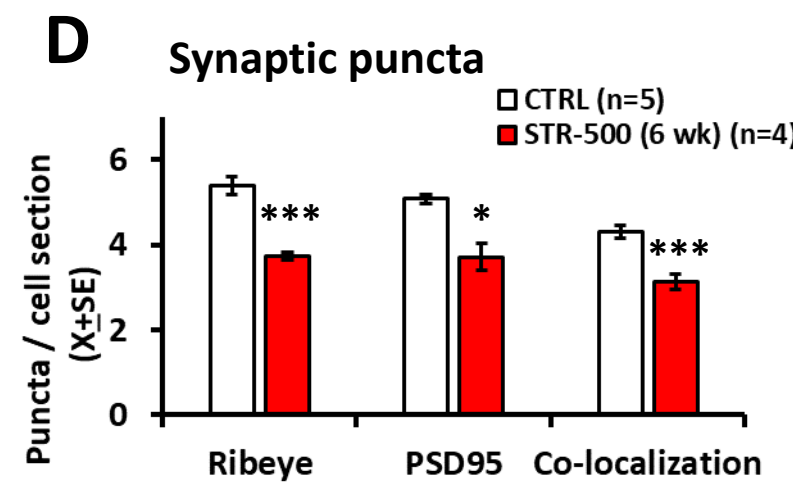
D
Synaptic puncta
CTRL (n=5)
STR-500 (6 wk) (n=4)
Puncta / cell section (X±SE)
6
4
2
0
***
*
***
Ribeye
PSD95
Co-localization

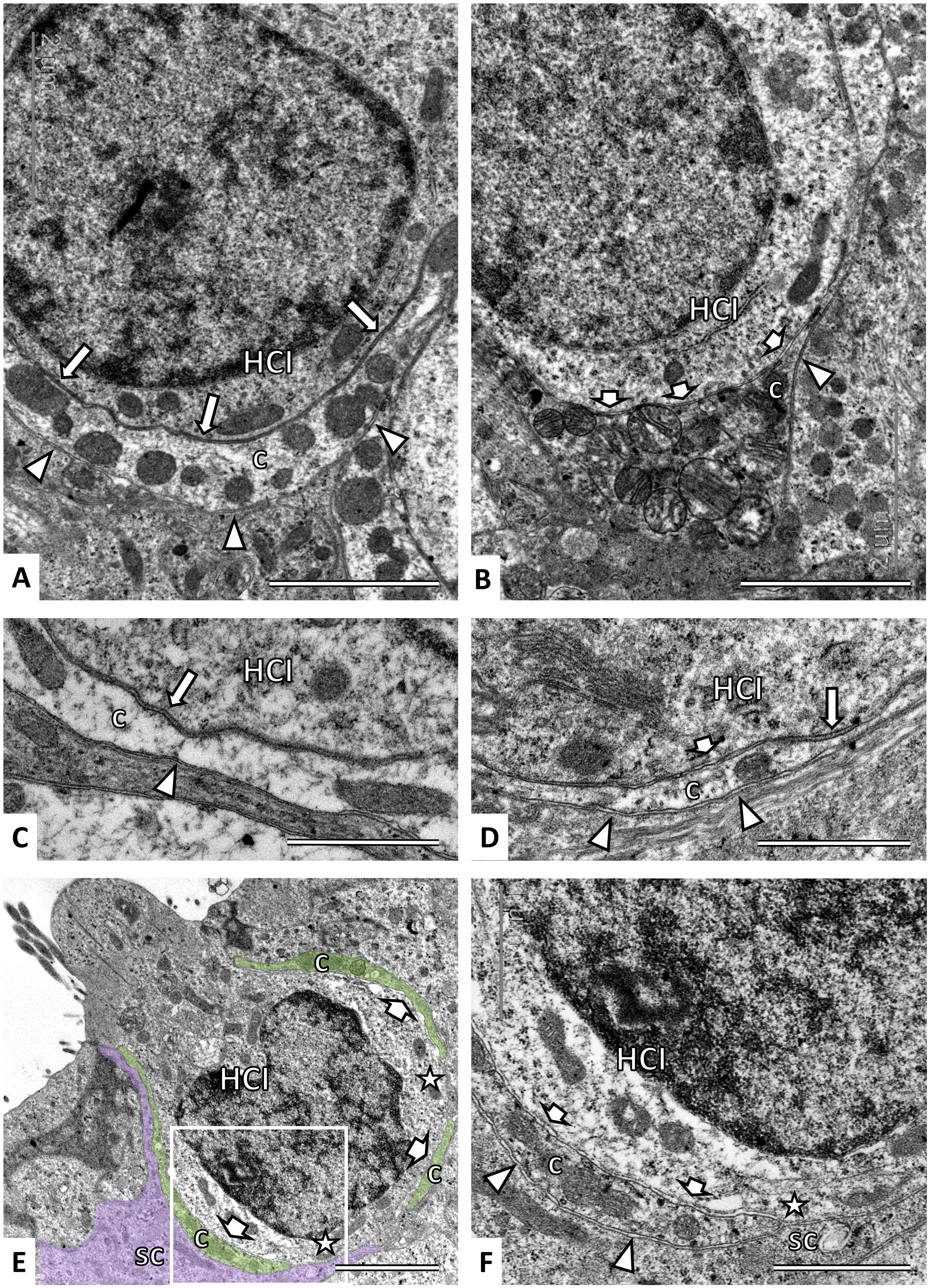
A
HCI
C
2 µm
B
HCI
C
2 µm
C
HCI
C
D
HCI
C
E
HCI
C
C
C
SC
F
HCI
C
SC

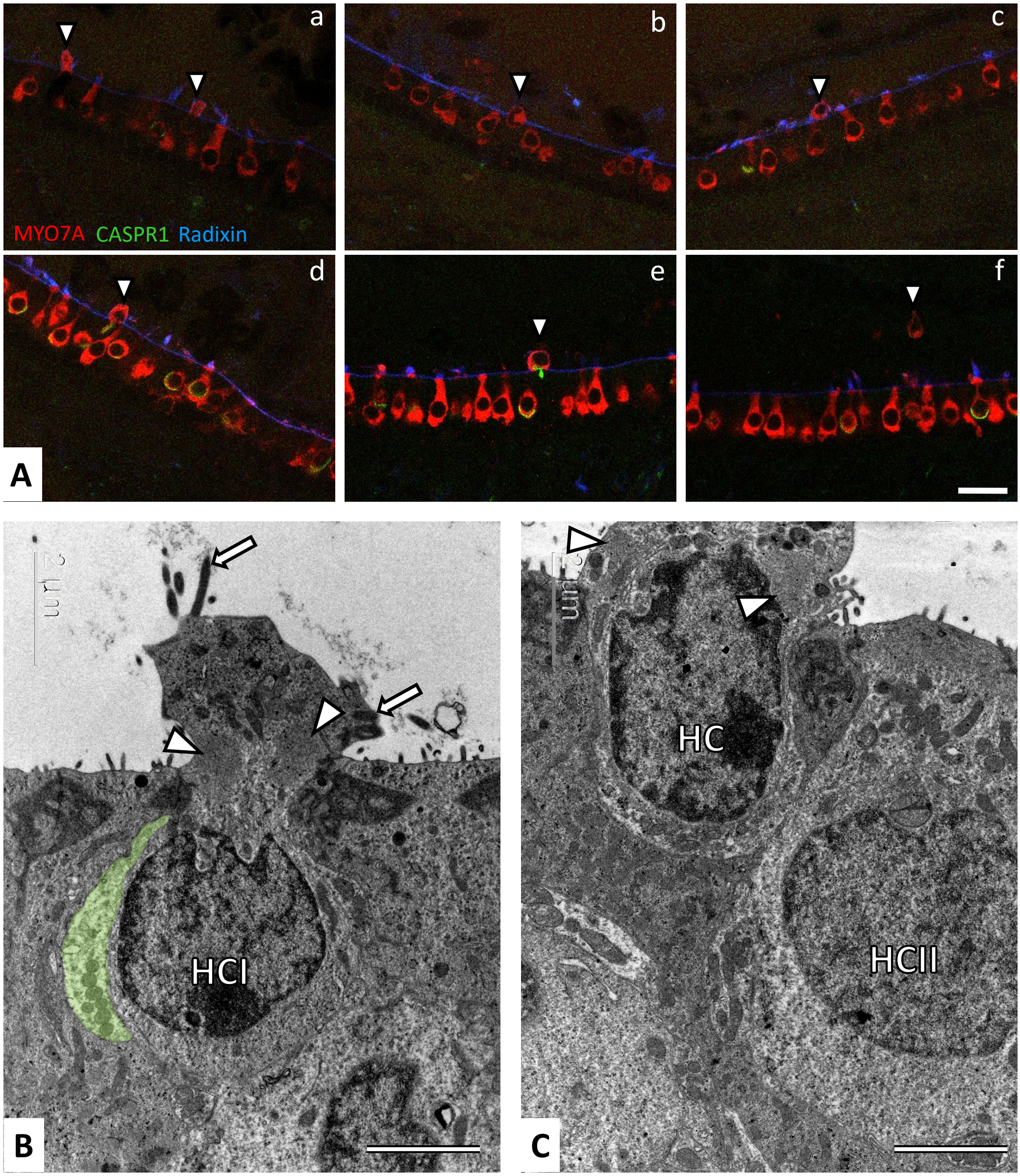
a
b
c
d
e
f
MYO7A CASPR1 Radixin
A
2 µm
HCI
B
3 µm
HC
HCII
C

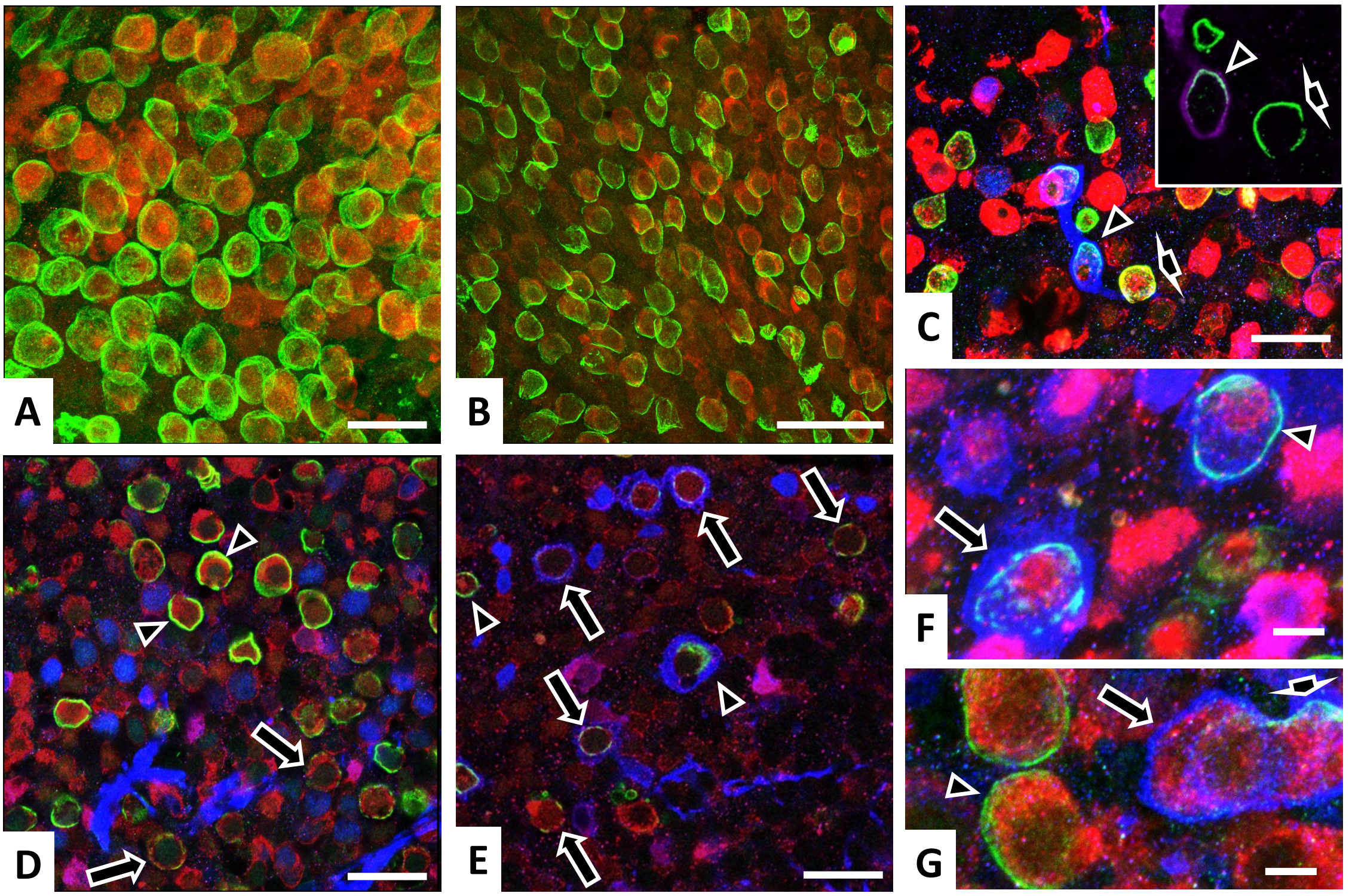
A
B
C
D
E
F
G